RSC Advances

REVIEW

View Article Online
View Journal | View Issue

Cite this: *RSC Adv.*, 2024, **14**, 16093

Architectural design and affecting factors of MXene-based textronics for real-world application

Md. Reazuddin Repon, *[abc] Daiva Mikučionienė, [c] Tamal Krishna Paul, [d] Jehan Y. Al-Humaidi, [e] Mohammed M. Rahman, [f] Tarekul Islam[dg] and Sharof Shukhratov[h]

Today, textile-based wearable electronic devices (textronics) have been developed by taking advantage of nanotechnology and textile substrates. Textile substrates offer flexibility, air permeability, breathability, and wearability, whereas, using nanomaterials offers numerous functional properties, like electrical conductivity, hydrophobicity, touch sensitivity, self-healing properties, joule heating properties, and many more. For these reasons, textronics have been extensively used in many applications. Recently, new emerging two-dimensional (2D) transition metal carbide and nitride, known as MXene, nanomaterials have been highly considered for developing textronics because the surface functional groups and hydrophilicity of MXene nanoflakes allow the facile fabrication of MXene-based textronics. In addition, MXene nanosheets possess excellent electroconductivity and mechanical properties as well as large surface area, which also give numerous opportunities to develop novel functional MXene/textile-based wearable electronic devices. Therefore, this review summarizes the recent advancements in the architectural design of MXene-based textronics, like fiber, yarn, and fabric. Regarding the fabrication of MXene/textile composites, numerous factors affect the functional properties (*e.g.* fabric structure, MXene size, *etc.*). All the crucial affecting parameters, which should be chosen carefully during the fabrication process, are critically discussed here. Next, the recent applications of MXene-based textronics in supercapacitors, thermotherapy, and sensors are elaborately delineated. Finally, the existing challenges and future scopes associated with the development of MXene-based textronics are presented.

Received 9th March 2024
Accepted 10th May 2024

DOI: 10.1039/d4ra01820f

rsc.li/rsc-advances

Introduction

In recent years, intense research growth has been seen in wearable technology due to fast-growing technological advancement.[1] The innovation of wearable electronic devices has changed our lifestyles due to their appealing applications in artificial intelligence,[2] human motion detection,[3] robotics,[4] energy storage systems,[5] human health monitoring,[6] and many more. Wearable electronic devices have some excellent intrinsic properties, like being lightweight, flexible, and easily attachable to the human skin, which has attracted scientists to develop a new generation of smart wearable devices. Impressively, textile substrates (*e.g.* fiber, yarn, or fabric) possess all these superior characteristics. Along with that textile materials show outstanding wash fastness, and physio comfort properties, like air-permeability, sweat absorption, *etc.* Therefore, textile substrates are now extensively used in developing wearable electronic devices. However, textiles are insulating materials. Therefore, it is needed to modify the textile's surface in order to prepare electronic textiles, which can also be called textronics. Regarding this, various conductive materials are used, for example, graphene,[7,8] carbon nanotube (CNT),[9] boron nitride,[10,11] metallic nanoparticles,[12] conducting polymer,[13,14] *etc.*

Among these electroactive materials, newly developed two-dimensional (2D) transition metal carbides and nitrides, also known as MXene nanomaterials, are widely used to fabricate MXene-based textronics. MXene nanomaterials are synthesized from MAX ($M_{n+1}AX_n$) phase precursors. Here, M is an early metal, A is a group IIIA or IVA element in the periodic table, X is carbon and/or nitrogen and the value of n is 1 to 3.[15] MXene

[a]*Department of Textile Engineering, Daffodil International University, Dhaka-1216, Bangladesh. E-mail: reazmbstu.te@gmail.com; Tel: +88-37066227098*

[b]*Department of Bioproducts and Biosystems, School of Chemical Engineering, Aalto University, 02150 Espoo, Finland*

[c]*Department of Production Engineering, Faculty of Mechanical Engineering and Design, Kaunas University of Technology, Studentų 56, LT-51424, Kaunas, Lithuania*

[d]*ZR Research Institute for Advanced Materials, Sherpur-2100, Bangladesh*

[e]*Department of Chemistry, College of Science, Princess Nourah Bint Abdulrahman University, P.O. Box 84428, Riyadh 11671, Saudi Arabia*

[f]*Center of Excellence for Advanced Materials Research (CEAMR) & Chemistry Department, Faculty of Science, King Abdulaziz University, Jeddah 21589, Saudi Arabia*

[g]*Department of Materials Science and Engineering, King Fahd University of Petroleum and Minerals, Dhahran, 31261, Saudi Arabia*

[h]*Department of Technological Education, Fergana State University, Fergana 150100, Uzbekistan*

nanoflakes are generally presented by the $M_{n+1}X_nT_x$ formula, where T_x represents the surface' functional groups such as –O, –OH, –F, and/or –Cl.[16,17] In 2011, Gogotsi and his co-workers first prepared Ti_3C_2 layered MXene with OH and/or F functional groups from Ti_3AlC_2 precursors by using hydrofluoric (HF) acid[18] and till now numerous MXene nanoflakes have been prepared, such as Ti_2C, V_2C, Nb_2C, Ti_4N_3, TiNbC, Ti_3CN, Mo_2TiC_2, *etc.*[19] 2D MXene nanosheets have excellent electrical, mechanical, and thermal properties along with high-temperature resistance and corrosion resistance characteristics, better than the other electroactive materials.[20,21] Due to these outstanding properties, research interests are grown in these 2D nanomaterials. Moreover, a large number of functional groups on the MXene surface allows an easy dissolution process in aqueous medium. Therefore, it is easy to deposit MXene materials on the textile substrate. The surface terminal groups of MXenes can form strong bonds with the textile substrate *via* hydrogen bonding. Cotton, for instance, has –OH functional groups which create strong adhesion bonds with MXenes functional groups. Furthermore, the functional groups of textile substrates and MXenes also allow additional surface modification to enhance the functional properties of MXene-based textronics. For instance, Wang *et al.* prepared MXene/PPy ink by *in situ* polymerization process before the dip-coating of poly(ethylene terephthalate) (PET) textiles.[22] Pyrrole solution was first introduced into MXene suspension and due to the acidic characteristics of MXenes, long polymer chains of polypyrrole (PPy) were formed with the MXene terminal groups. After that PET textile, pretreated with NaOH, was dipped into MXene/PPy stable ink. Furthermore, silicone coating was introduced on MXene/PPy@PET textiles to make the hydrophobic surface, which solved the oxidation problems of MXene as well as enhanced the wash fastness properties. Thus, it is

Md. Reazuddin Repon

Dr Md. Reazuddin Repon is a Researcher at Nature Research Centre, Vilnius, Lithuania. He received his PhD in Materials Engineering from Kaunas University of Technology, Kaunas, Lithuania. He received his BSc and MSc in Textile Engineering from Mawlana Bhashani Science and Technology University, Bangladesh. He also holds positions as a Researcher in the Faculty of Mechanical Engineering and Design at Kaunas University of Technology in Lithuania, a Visiting Researcher in the Department of Textile Engineering at Daffodil International University in Bangladesh, and an Adjunct Faculty member in the Department of Textile Engineering at Khwaja Yunus Ali University in Bangladesh. He also worked as a Junior Researcher in the Department of Production Engineering at Kaunas University of Technology, Lithuania and Senior Lecturer in the Department of Textile Engineering at Khwaja Yunus Ali University, Bangladesh. His research interests include wearable and flexible electronic textiles, smart clothing systems, functional materials, fibre reinforced composites, and eco-friendly and sustainable textile coloration.

Daiva Mikučionienė

Prof. Dr Daiva Mikucioniene obtained her PhD, MSc and BSc degrees from Kaunas University of Technology (KTU), Kaunas, Lithuania. She has worked in KTU for more than 20 years. Presently, she is working as Professor in the Department of Production Engineering, Faculty of Mechanical Engineering and Design, KTU, Lithuania. Areas of her interest are medical and protective textiles, theoretical modelling and development of knitted structures, and electronic wearables. She has published more than 60 papers in international journals with IF from the list of Web of Science (WoS) database, and is author and co-author of 12 edited books for students. She is a member of Editorial Board of 2 international scientific WoS journals – Autex Research Journal and Fibres and Textiles in Eastern Europe; recently has been a member of several international scientific conferences. She is a member of KTU Doctoral Committee Materials Engineering; she was a member (or chairperson) of more than 20 international Dissertation Defense Boards. She has supervised 12 PhD students (8 of them already successfully graduated). She is a member of Council of the Faculty of Mechanical Engineering and Design, KTU, member of Committee of study programs in the field of Polymers and Textile Technology, Coordinator of Mentorship program of the Faculty of Mechanical Engineering and Design. She has a deep experience in coordination and implementation of international and national projects in the field of Materials Engineering, Textiles. She is awarded by honour award "Gold Spindle" of Lithuanian Apparel and Textile Industry Association (LATIA) for "merits of developing of Lithuanian apparel and textile industry".

Tamal Krishna Paul

Tamal Krishna Paul is currently working as a Junior researcher at ZR Research Institute for Advanced Materials (ZRRIAM), Bangladesh. He completed his undergraduate degree in Textile Engineering from Khulna University of Engineering & Technology, Khulna, Bangladesh. He also worked as a Research Assistant at the Laboratory of Nano-bio and Advanced Materials Engineering (NAME) at Jashore University of Science and Technology, Bangladesh. His research interests lie in synthesizing nanomaterials and developing their novel functional materials for advanced sensing and energy storage applications.

Prof. Dr Jehan Y. Al-Humaidi received her PhD from Princess Nourah University, Saudi Arabia in 2010 in Organometallic Chemistry. Currently she is working as professor in the Princess Nourah Bint Abdulrahman University, Riyadh, Saudi Arabia. Her research interests include Organic Synthetic Methodology, Polymers, Enzymes, Drugs, Polymeric materials, Natural products, and Nanocomposites, etc.

Mohammed M. Rahman

Prof. Dr Mohammed M. Rahman is Professor of Chemistry Department with CEAMR Research-Center at King Abdulaziz University, Saudi Arabia since February 2019. Before joining King Abdulaziz University as an Assistant Professor in 2011, he served for two years as an Assistant Professor in the Department of Chemistry (with CAMNE Research-Center) at Najran University. He completed his BSc (Chemistry; 1999) and MSc (Physical Chemistry; 2002) from Shahjalal University of Science & Technology, Sylhet, Bangladesh. He received his PhD degree from Chonbuk National University, South Korea in 2007. Before becoming an academician, he worked as a Postdoctoral research fellow at Pusan National University (2007/2008, South Korea) and Toyohashi University of Technology (2008/2009, Japan) consecutively. He published many research articles in peer-reviewed journals, US patents, book chapters and books. He serves as Editorial board member in various international journals. His research interests are in the field of Material Science, Nanotechnology, Conducting Polymers, Bio- & Chemo-Sensors, Nanocomposites, Carbon Nanotubes, Photocatalysis, and Smart Micro- & Bio-chips.

Tarekul Islam

Tarekul Islam is currently pursuing his MS program in Materials Science and Engineering at King Fahd University of Petroleum and Minerals, Saudi Arabia. He works as a Head of the Department of Research and Innovation at ZR Research Institute for Advanced Materials, Sherpur-2100, Dhaka-Bangladesh. He completed his undergraduate degree in Textile Engineering from Mawlana Bhashani Science and Technology University, Tangail, Dhaka-Bangladesh. He also worked as a Lecturer in the Department of Textile Engineering at Khwaja Yunus Ali University, Bangladesh. His research interests are in nanomaterials, protective materials, sensor, electrospinning, and wearable flexible electronics.

possible to fabricate MXene-based textronics with different functional properties according to the requirements, thanks to the adjacent functional groups of both textile materials and MXene nanomaterials. For these numerous advantages, MXene-modified textronics are commonly used in electromagnetic shielding, energy storage systems (*e.g.*, wearable supercapacitors and batteries), medical fields (*e.g.*, ECG, wearable thermotherapy, *etc.*), defense (*e.g.*, body armour), and many other fields.

Although MXene shows its dominance in developing textile-based wearable devices over other conductive counterparts, it needs to pay attention to the fabrication strategies of MXene-based textronics. Because MXene nanosheets tend to aggregate due to the van der Walls force between the MXene flakes, causing the degradation of functional properties. Also, MXenes show oxidation problems. As a result, the concentration of MXene solution, amount of MXene deposition on the textile substrate, and many more factors should be carefully selected. Therefore, it is urgent to outline the overall performance of MXenes in fabricating the MXene-based textronics. For instance, Meena *et al.* described the surface properties of $Ti_3C_2T_x$ MXenes, fabrication techniques of smart textiles using MXenes, and the applications of MXene-based textronics.[23] Zhang *et al.* presented the synthesis process of MXenes, the fabrication process of MXene-based textiles, and their performance in supercapacitor applications.[24] However, to the best of our knowledge, no study has been found that extensively focuses on the affecting parameters for enhancing the functional properties of MXene-based textronics. MXenes flake size and concentration, surface modification of MXenes and textile materials by carefully chosen materials, different types of fiber and the fabric greatly affect the properties of MXene-based textronics. It is urgent to elaborately discuss these parameters. Therefore, we focus on this topic in this paper. At first, an elaborate discussion has been presented to fabricate MXene-based textronics. Then the effect of different parameters, like fabric structures, fiber types, MXene size, and others on the

Sharof Shukhratov

Dr Sharof Shukhratov is an Associate Professor of Technology Education Department at Fergana State University, Uzbekistan. He received his PhD in Materials Engineering from Kaunas University of Technology, Kaunas, Lithuania. He received his BSc and MSc from Tashkent Institute of Textile and Light Industry, Tashkent, Uzbekistan. His research interest includes wearable and flexible electronic textiles, functional materials, fibre reinforced composites, mechatronics and robotics systems, cotton waste cleaner and the methods of parameters and operation modes of spinning.

functional properties of MXene-based textronics are reviewed. Finally, the potential applications of such fabricated MXene-based textronics are discussed.

Structural design of MXene-based textronics

Coating

Coating is one of the most convenient ways to fabricate MXene-based conductive yarn. The coating technique mainly involves the deposition of a thick layer of desired materials on the substrate's surface so that the properties of the substrate, like mechanical, electrical, thermal, chemical, and so forth, can be significantly improved. There are numerous coating approaches (*e.g.* dip coating, spray coating, *in situ* polymerization, drop-casting, and spin coating). Regarding the uniform MXene coating on the textile substrate, the preparation of MXene dispersion stages, such as the selection of the proper solvent, MXene flake size, and concentration, play a critical role.[25] In addition, the number of coating layers is very important, because an excess amount of MXene materials on the textile substrate may cause aggregation, which may deteriorate the desired performances. Therefore, coating layers should be properly maintained. The interaction of MXene nanosheets and the textile substrates mainly occurs through hydrogen bonding between the MXene surface functional groups and the substrate's polarity.[26] To ensure good adhesion properties, cellulosic fabric or yarn surface is pretreated with acetone, ethanol, and NaOH to activate the functional groups. Furthermore, for MXene coating on hydrophobic fabric or yarn surface, plasma treatment is the common approach, because this process creates functional groups like hydroxyl, amide, carbonyl, or carboxylic acid on the substrate's surface.[27] Thus, the hydrophobic surface turns into a hydrophilic stage. The subsequent subsection provides an in-depth discussion of MXene coating approaches to fabricate wearable textronics.

Dip coating. Dip coating technique is one of the simplest processes for MXene loading on the fabric or yarn surface. In this process, the fabric or yarn substrates are dipped into the MXene solution for several minutes.[28] Then the substrate is dried in air or put in an oven drier under a certain temperature. This dipping and drying process can be repeated several times to increase the MXene amount on the surface. In addition, the thickness of the coating layer can be controlled by this technique. For instance, Wang *et al.* fabricated MXene-modified core–sheath elastic yarn (CSY).[29] For preparing CSY, polyurethane filament and polyester filament were fed into a roller simultaneously, which were then twisted together to obtain the yarn. The CSYs were ultrasonicated in water to remove wax and impurities. After that, the CSYs were dipped into MXene solution for 10 minutes, followed by drying at 120 °C in an oven for 10 minutes. Liu *et al.* used polymeric textiles, poly(ethylene terephthalate) (PET), to load MXene nanosheets by dip coating approaches.[30] Prior to that the polymeric textile surface was treated with strong alkali (NaOH) solution at 80 °C for 2 hours. For NaOH treatment, the ester group of PET textiles is broken, resulting in oxygen functional groups. Therefore, after dipping alkali-treated PET textiles into MXene dispersion, strong interfacial interaction occurred between the surface functional group of MXene and PET textiles. Moreover, the dip coating technique allows large-scale production of MXene-based textronics because of its easy fabrication process. It has been seen that cotton rovings were immersed in MXene dispersion for 30 minutes followed by drying.[31] Then the electroactive stretchable yarn was fabricated by spinning MXene/cotton rovings and spandex yarn with the spinning speed of 900 m h^{-1}. This demonstrated the industrial scalability of MXene-based textronics.

***In situ* polymerization.** The *in situ* polymerization technique allows the polymerization process on the fabric surface instead of initiating the polymerization separately. The uniform deposition of polymeric materials on the substrate's surface is the main advantage of *in situ* polymerization. Thus, it ensures proper bonding strength between the polymer and fiber. Modification of MXene-treated fabric by *in situ* polymerization technique involves the following steps: (1) MXene-modified fabric or yarn will be dipped into a monomer solution; (2) an oxidant solution will be added to the MXene-treated fabric or yarn surface to start the polymerization process. For instance, Yang *et al.* fabricated PPy/MXene@cotton (PMCF) yarn.[32] At first, they soaked cotton yarn in a mixture of pyrrole (Py) and MXene solution. Then to initiate the polymerization, 1 wt% $C_{14}H_7NaO_5S$ and 4 wt% $(NH_4)_2S_2O_8$ were used. The fabrication process is described in Fig. 1(a). The fabricated yarn showed excellent mechanical strength and electrical conductivity, 107.3 MPa and 60.8 S m^{-1} respectively. Li *et al.* used Py monomer for *in situ* polymerization.[33] Before polymerization, they modified the fabric with positively charged polyethyleneimine (PEI) and negatively charged $Ti_3C_2T_x$ MXene nanosheets. Therefore, electrostatic interaction occurred between PEI and MXene nanosheets. After that MXene/PEI-modified fabric was soaked into pyrrole/*p*-toluenesulfonic acid (PTSA) dispersion, followed by dropping $FeCl_3 \cdot 6H_2O$ (0.87 g) oxidant solution to initiate the polymerization. In another study, it has been seen that aniline monomer was used for the polymerization to modify the carbon fiber fabric (CF).[34] Prior to that, the CF was pre-treated with HNO_3 solution. Therefore, a large number of oxygen-containing polar groups and positive charges were induced, which favored the MXene loading on the fabric surface. Then MXene/CF was dipped into aniline monomer solution. To deposit the polyaniline (PANI) layer on MXene/CF fabric, APS oxidant was added. PANI exhibited positive zeta potential (+18.9 mV); therefore, strong interfacial bond occurred between negatively charged MXene and positively charged PANI.

Although the *in situ* polymerization process allows uniform deposition of polymeric materials on a bulk scale, this process doesn't allow the control of the thickness of electroactive materials on the substrate. In addition, as the monomer solution needs to be deposited on the substrate at first, after polymerization the aggregation of polymer materials may be introduced. Furthermore, there may exist unreacted monomer due to not controlling over polymerization process. For these

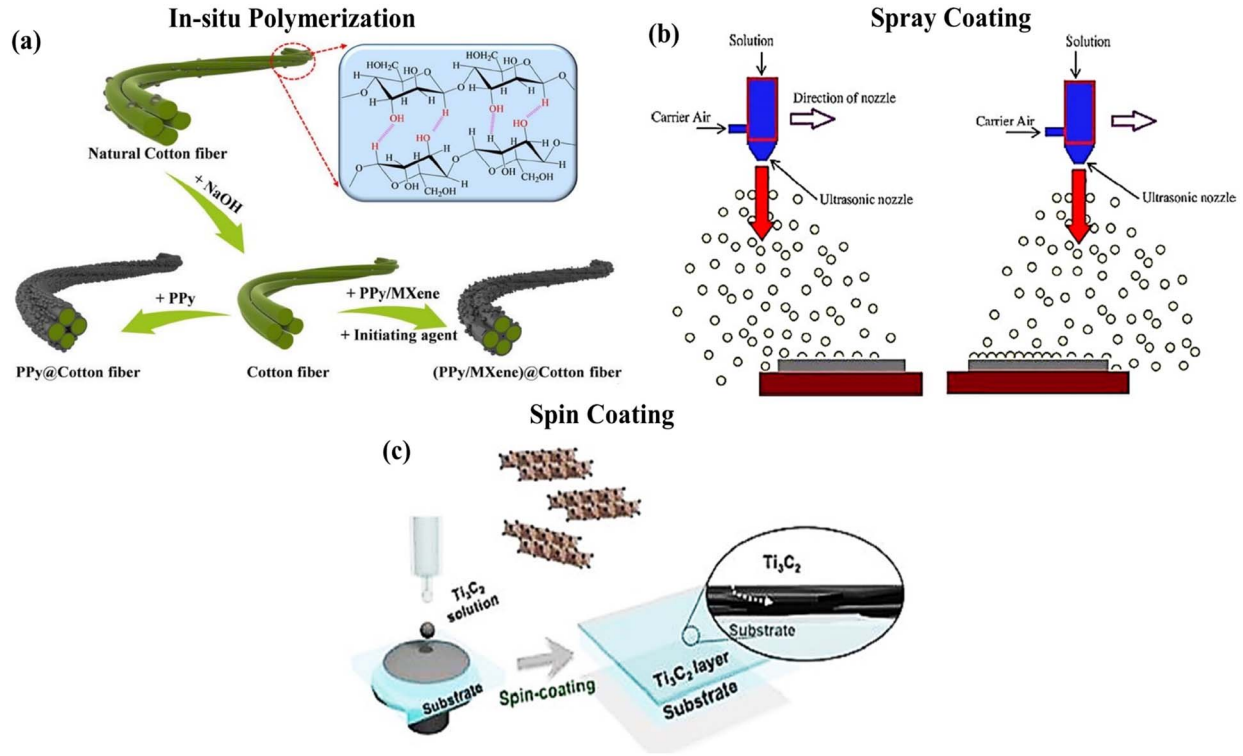

Fig. 1 (a) *In situ* polymerization process pyrrole monomer. Reproduced with permission.[32] Copyright©2021, Elsevier. (b) Spray coating approach. The coating layer is increased over time. Reproduced with permission.[36] Copyright©2015, Elsevier. (c) Spin coating technique of MXene nanomaterials. Reproduced with permission.[43] Copyright©2020, Wiley.

reasons, the concentration of monomer and oxidant for the polymerization process needs to be selected very carefully.

Spray coating. Spray coating of MXene nanomaterials involves the spraying of MXene solution inks on the textile substrate through a nozzle under a certain pressure.[35] After spraying, the textile substrates are dried, subjecting the evaporation of liquid materials and allowing the dried MXene nanosheets to adhere to the substrate. Fig. 1(b) shows a schematic illustration of the spray coating process at two different times.[36] This technique is widely used in art and industries. Large-scale production can be achieved by using the spray coating process because it requires less time to deposit the active materials on the substrate.[37] Moreover, thin deposition of active materials on the substrate is achieved within a very short time. In addition, the thickness of the coating layer can be controlled by adjusting several parameters, the distance between substrate and nozzle, air pressure, and solution concentration.[38] Generally, it has been seen that the MXene concentration for spray coating is kept between 0.1 mg ml^{-1} to 10 mg ml^{-1}.[39] For instance, 4 mg ml^{-1} of MXene solution was used for spray coating at a pressure of 4–6 psi through a 0.3 mm nozzle on polyethylene terephthalate substrate.[40] With this spraying condition, the thickness of the coating layer was achieved at 0.78 μm, which showed an excellent shielding efficiency of 50 dB. Although the spray coating technique is scalable, the wastage of materials is high in this technique.

Spin coating. In spin coating, the desired solution is dropped on the substrate and then the substrate is rotated for a certain time to deposit the coating materials, followed by evaporating the solvent.[41] The main advantage of spin coating is its capability of depositing coated materials homogeneously on the substrate. However, there will be more solution wastage (almost 80–90%).[42] Fig. 1(c) shows the process of spin coating of MXene nanomaterials.[43] The thickness of the coated layer can be controlled by the applied shear force and the duration of the coating.[44] For instance, rGO/Ti_3CNT_x film was fabricated *via* spin-coating techniques.[45] At first, 60 μl of Ti_3CNT_x solution was deposited on a glass substrate which was rotated at 2000 rpm for 30 seconds. The thickness of the film was controlled by varying the spin cycles. After that 120 μl of GO/L-ascorbic acid (LAA) was added to the previous Ti_3CNT_x film at 2000 rpm for 30 seconds. After the spinning, the sample was placed at 150 °C for 20 minutes to reduce the GO as well as to obtain the rGO/Ti_3CNT_x film. The obtained film exhibited a sheet resistance of about 19 kΩ sq^{-1}. In another study, it has been seen that Cu–Ni alloy-coated nylon textile was used as the substrate for spin-coating of MXene/PDMS mixture, which was cured at 80 °C for 2 hours.[46] Although, the spin-coating technique ensures a homogenous distribution of the materials, the thickness and homogeneity of the coating layer may be disrupted by changing the spinning speed.[47] Another major disadvantage of spin-coating is the size of the substrate, which hinders the scalable production. Moreover, increasing the size of the substrate makes it almost difficult to obtain high-speed spinning performance.[48]

Furthermore, during the vaporization of the solvent, high temperature may weaken the fabric strength, which can deteriorate the fabric's performance.

Electrospinning

The electrospinning technique is widely recognized as one of the most efficient techniques to fabricate nanofiber in non-woven form. Electrospinning involves three main basic components: (1) a high voltage supplier, (2) a spinneret, and (3) a collecting screen.[49] In the electrospinning process, when high voltage is applied, the polymer solution comes out from the spinneret and is stored on the collecting screen. Before reaching to collecting screen, the polymer solution is solidified.[50,51] On the collecting screen, the nanofiber is obtained in a non-woven web form, which has a high surface area-to-volume ratio. During the fabrication of electrospun fiber, the spinneret is exposed to the applied electric field, which creates a charge on the surface of the liquid.[52] Increasing the applied voltage forms a conical shape of the liquid at the tip of the spinneret, which is known as the Taylor cone and further increasing the voltage helps to overcome the surface tension.[52,53] Finally, the charged liquid is ejected from the Taylor cone and deposited on the collector. Fig. 2(a) shows a schematic illustration of the horizontal setup of the electrospinning apparatus.[49] As high electric voltage is applied for electrospinning, loading high conductive liquids may result in short circuits, which may deteriorate the performance.[25] To solve this shortcoming, carbonization of the nanofiber can be effective. It is seen that MXene/PAN electrospun nanofiber was carbonized to increase the conductivity in order to obtain better supercapacitive performance.[54] Before the carbonization process, the MXene/DMF solution was centrifuged to collect the MXene sediment, which was then added to the PAN/DMF solution and finally, the solution mixture was stirred overnight to prepare the spinning solution. The spinning solution was poured into the spinneret and then the

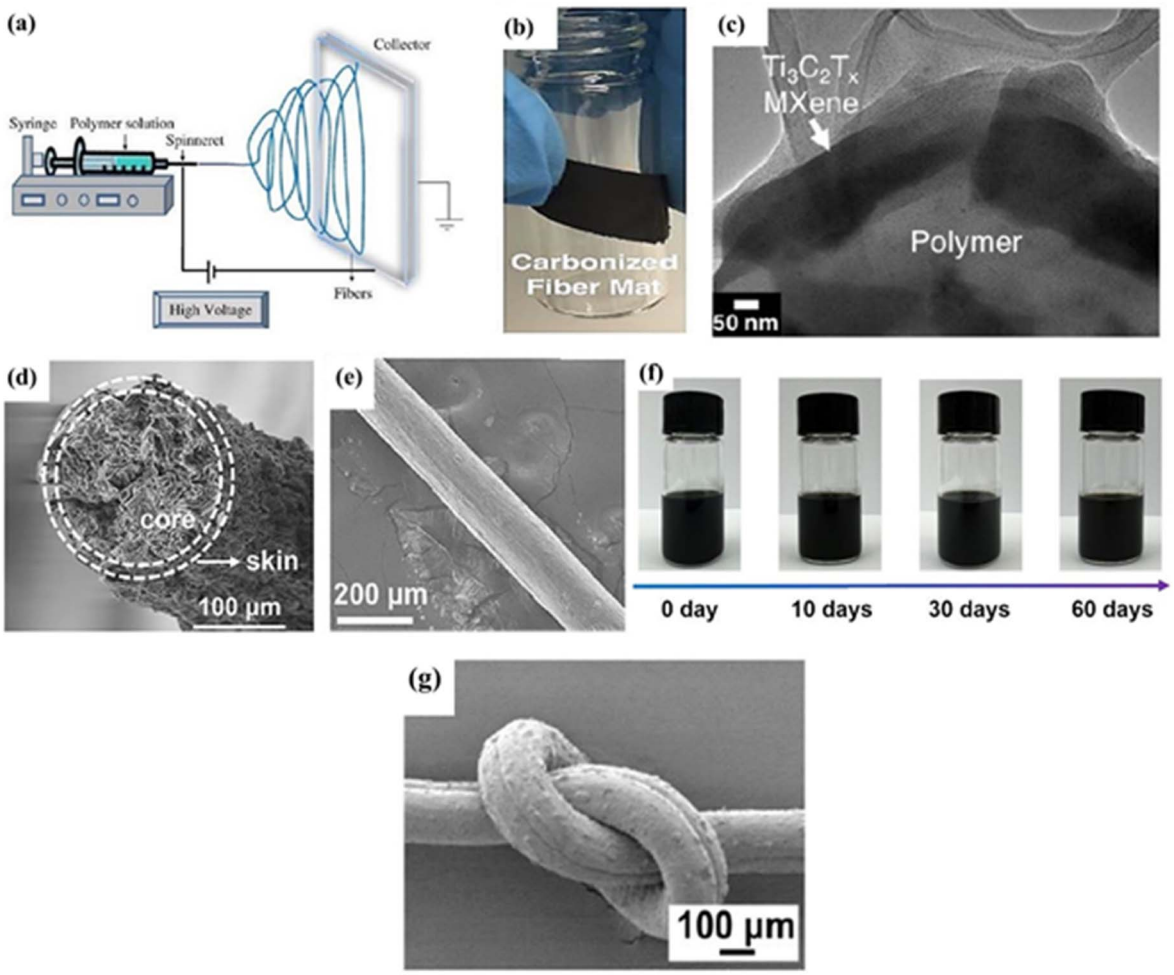

Fig. 2 (a) Schematic illustration of horizontal electrospinning approach. Reproduced with permission.[49] Copyright©2010, Elsevier. (b) MXene/PAN carbonized electrospun nanofiber wrapped around a glass vial, demonstrating its superior flexibility.[54] (c) The electrospinning process allows uniform distribution of MXene nanomaterials in a polymer matrix. Reproduced with permission (b and c).[54] Copyright©2019, The Royal Society of Chemistry. (d) Core–skin structure of wet-spun Kevlar/MXene fiber.[62] (e) Smooth and homogenous surface of wet-spun Kevlar/MXene fiber. Reproduced with permission (d and e).[62] Copyright©2021, American Chemical Society. (f) Stable MXene/silk wet-spinning solution.[64] (g) Knitted MXene/silk wet spun fiber, demonstrating its superior flexibility. Reproduced with permission (f and g).[64] Copyright©2023, American Chemical Society.

voltage was applied. Finally, the nanofiber mat was collected and carbonized to prepare MXene/PAN carbonized composites. The obtained nanofiber mat showed higher flexibility, as demonstrated in Fig. 2(b). In addition, Fig. 2(c) exhibits the homogenous interconnection of MXenes along the fiber axis. In another study, it has been found that $Ti_3C_2T_x$-MXene/poly(vinylidenefluoride-cotrifluoroethylene) (P(VDF-TrFE)) nanofibers prepared *via* electrospinning process.[55] For this, MXene/DMF solution and P(VDF-TrFE)/DMF/acetone solution were transferred into a syringe with 15 kV applied voltage. Then the nanofiber was obtained on the aluminum foil paper. To increase the conductivity, the nanofiber film was further dipped into MXene solution.

MXene nanomaterials have wide surface functional groups and for this reason, MXene can be dispersed in a wide variety of polar solvents, such as chitosan,[56] poly(acrylic acid) (PAA),[57] poly(ethylene oxide) (PEO),[57,58] poly(vinyl alcohol) (PVA),[57] and alginate/PEO.[57] However, during the electrospinning process, one should be very careful, as there is a high applied voltage, which may cause electric shock. In addition, several parameters, such as solution viscosity, the amount of MXene loading, applied voltage, the distance between the spinneret and collector, temperatures, and many more, should be chosen carefully.

Wet spinning

Wet spinning, nowadays, has gained enormous attention regarding the fabrication of flexible yarn, that can be woven or knitted into garments for the production of smart wearable devices. To fabricate yarn by wet spinning, four steps are followed: (1) dissolution of polymer materials, (2) extrusion of the polymer solution from the spinneret, (3) coagulation, and (4) collection of the yarn.[59] A polymer solution is typically extruded from the spinneret to the coagulation bath, where the polymer solution begins to solidify.[60] After that, the yarn is washed and collected on a rotating beam. Regarding the wet spinning process, several parameters, like the rheological properties of polymer solution, solvents in the coagulation bath, spinneret diameter, winding speed, and processing temperature, play important roles.[59] By using this technique, it is possible to produce continuous yarn which is, nowadays, highly demandable for wearable electronic devices. For the wet spinning of MXene materials, the main challenge is to control the weak interlayer connection between the MXene nanosheets. Introducing additional materials as binders may solve this challenge. However, the mass ratio of active materials and the binders should be chosen very carefully so that the two components can't adversely affect the desired properties of the fabricated yarn. In addition, it is also important to carefully choose the solvent of the coagulation bath. Otherwise, the desired properties of the yarn cannot be obtained. In this case, the coagulant solvent should be nonsoluble for both the components of the hybrid materials. In this section, different materials that are used as additive binders with MXene during the wet-spinning process are mentioned accordingly.

Wet spinning of MXene/polymer blends. Zhang *et al.* used PEDOT:PSS as a conductive binder with $Ti_3C_2T_x$ to produce wet-spun fiber.[61] The wet-spun MXene/PEDOT:PSS fiber showed a high conductivity of 1489 S cm^{-1} with 70 wt% of MXene loading. Regarding the wet-spinning process, MXene/PEDOT:PSS spinning solution was passed through the coagulation bath containing sulphuric acid (H_2SO_4) and then washed with a water/ethanol mixture, followed by drying. Introducing MXene resulted in removing the π–π stacking of PEDOT, addressing the well-aligned MXene nanosheets into PEDOT:PSS. In addition, the intense peak of MXene for both 50 wt% and 70 wt% loading proved the presence of MXene flakes with PEDOT:PSS. Cheng and Wu used Kevlar fiber as the reinforcing agent with $Ti_3C_2T_x$-MXene for wet-spinning.[62] Kevlar fiber was exfoliated with methanesulfonic acid (MSA) and trifluoroacetic acid (TFA) to make Kevlar acid solution. Then MXene was dispersed with the Kevlar acid solution homogenously to prepare the Kevlar/MXene (KM) spinning dope. KM solution was extruded through a spinneret into an acetic acid bath solution which was dried in air and collected on a bobbin. Fig. 2(d) and (e) show the core–skin structure and homogenous surface of the KM fiber respectively, proving the successful preparation of Kevlar/MXene wet-spun fiber. In a similar study, it has been seen that aramid nanofiber (ANF)/DMSO solution and $Ti_3C_2T_x$-MXene/DMSO solution were used for spinning dopes.[63] The ANF/DMSO and MXene/DMSO were placed separately in two needles. Then the spinning dopes were extruded into the coagulation bath at a constant speed of 0.03 ml min^{-1}. The extruded fibers were solidified due to the interaction of coagulant solvent, $DMSO/H_2O/CH_3COOH$. The resultant fiber showed a high mechanical strength of 130 MPa. In MXene/ANF wet-spun fiber, aramid acted as the high-strength frame around the MXene layer due to the connection of ANF with the coagulant bath. Furthermore, the hydrogen bond between the MXene's hydroxyl group and the amide bonds of aramid made the MXene/ANF fiber a robust structure. Besides the use of synthetic polymeric fiber, it has also been noticed that naturally abundant polymers, such as silk, cellulose, alginate, chitosan, and many others, are widely used with MXene materials because good interfacial interaction between MXene and natural polymer can be achieved *via* hydrogen bonding. Furthermore, MXene/natural polymer composite ensures biodegradability, biocompatibility, and carbon footprint reduction. In addition, the synthetic polymer fiber can't ensure proper air permeability. Therefore, the use of natural polymer with MXene nanomaterials is increased day by day to fabricate soft, flexible, wearable electronic devices. For instance, Yue *et al.* used silk fibroin as the biotemplate with MXene nanosheets to fabricate degradable, stretchable wet-spun fiber.[64] For the wet-spinning process, MXene dispersion and silk solution were mixed, which showed no agglomeration or precipitation even after 60 days, as demonstrated in Fig. 2(f). The spinning solution was transferred into $(NH_4)_2SO_4$ containing a coagulation bath, and the fibers were rolled at a speed of 10 rpm. Furthermore, the fibers are additionally passed through the $CaCl_2$ bath to increase the toughness of the fiber. Fig. 2(g) shows the knitted structure of the produced fiber, demonstrating flexibility, stretchability, and softness which is favorable for the fabrication of wearable electronic devices. Furthermore, it has also been seen that crystalline nanocellulose (CNC) was used

with $Ti_3C_2T_x$-MXene nanomaterials to induce liquid crystalline behavior for the fabrication of wet-spun fiber.[65]

Wet spinning of MXene/carbonaceous materials. Seyedin *et al.* used liquid crystal (LC) graphene oxide with $Ti_3C_2T_x$-MXene nanosheets to fabricate the yarn.[66] They prepared the spinning solution by using sequential centrifugation to increase the MXene loading as well as to preserve the LC behavior. In addition, they used acetic acid as the coagulant solvent to produce the high-strength fiber. Fig. 3(a) shows the knitted MXene/GO fiber and knitted structure respectively, proving the flexibility of the MXene/GO wet-spun fiber. Zhao *et al.* fabricated $Ti_3C_2T_x$-MXene/CNT wet-spun fiber with 1 wt% loading of CNT.[67] To prepare the homogenous spinning dopes, CNT was first added into sodium taurodeoxycholate (STDOC) to make CNT dispersion, inducing a negative charge on CNT. Thus the repulsion occurred between the negatively charged CNT and MXene nanomaterials which resulted in homogenous spinning solutions. Fig. 3(b) shows the cross-sectional image of MXene/CNT nanofiber with no agglomeration. In addition, from Fig. 3(c), it has been noticed that the mechanical toughness was increased with the increased amount of CNT due to the strong interconnection between CNT and MXene, which was much higher than the pure MXene fiber.

Furthermore, under stress conditions, as shown in Fig. 3(d), CNT stretched along the fiber axis, which ensured the mechanical toughness of the wet-spun fiber. For the practical application of smart textiles, the conductive yarn must be highly stretchable because textile-based wearable devices undergo different bending conditions for daily uses. For this purpose, Wu *et al.* used thermoplastic polyurethane (TPU) as the polymer framework and MXene/CNT as the conductive networks.[68] For preparing the wet-spinning solution, MXene/DMF suspension was prepared in which CNT was added, followed by stirring to make MXene/CNT dispersion. Then TPU was added into MXene/CNT and stirred the solution at 70 °C to prepare the final spinning dopes. CNTs/MXene-TPU spinning dispersion was injected into a coagulation bath containing water to solidify the fiber. In the coagulation bath, DMF was rapidly diffused, resulting in the formation of MXene/CNT-TPU fibers. Moreover, Zheng *et al.* used sodium hyaluronate (HA) as the dispersant to ensure the uniform dispersion of MXene and CNT for the spinning solution. HA acts as the protective layer to remove the restacking problem of MXene and CNT. In addition, 75% ethanol-$CaCl_2$ was used in a coagulation bath to solidify the fiber.[69]

Wet spinning of pure MXene-based fiber. Wet spinning of pure MXene fiber is challenging because there are some problems in processing MXenes, like weak interlayer connection, oxidation, and many more. To solve this issue, Eom *et al.*, for instance, developed a new method to fabricate wet-spun MXene fiber without using any binder or additives.[70] $Ti_3C_2T_x$-MXene was prepared by etching the Al layer from Ti_3AlC_2 precursors.

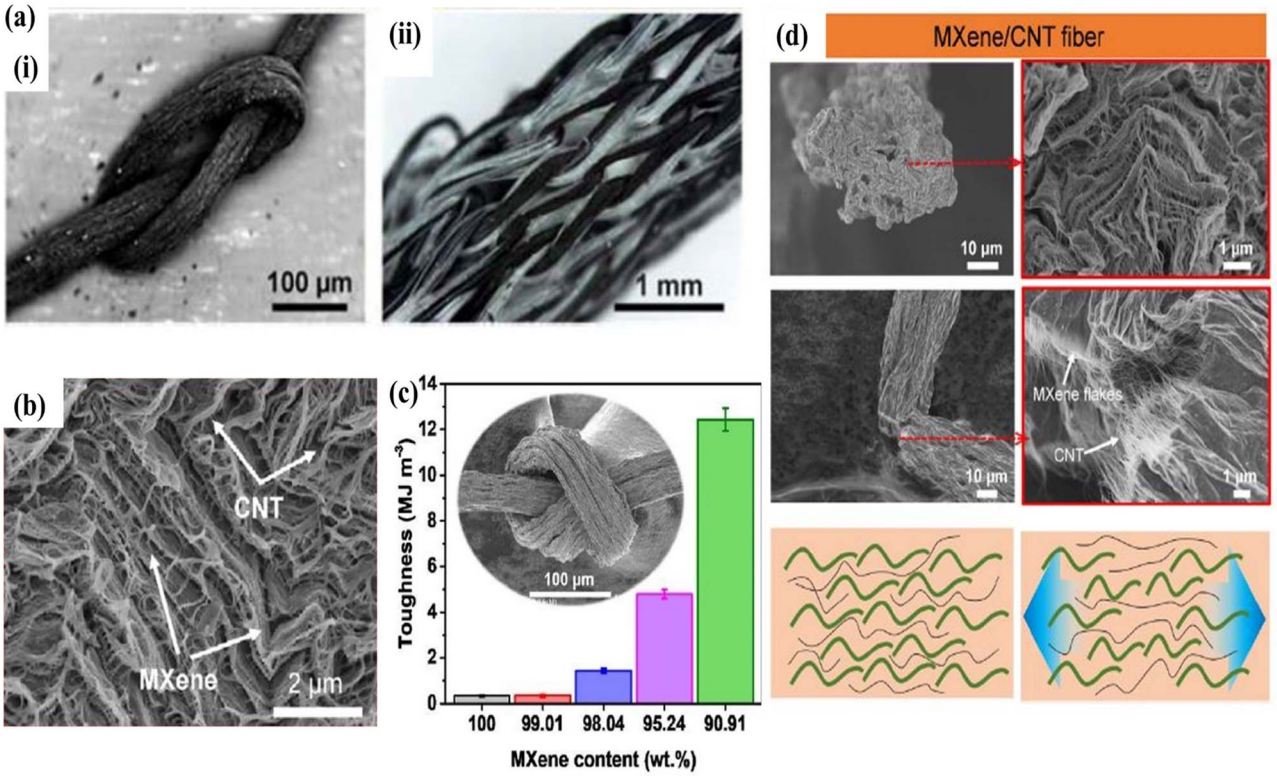

Fig. 3 (a) The wet-spun MXene/GO fiber can be knitted due to its high flexibility. Reproduced with permission.[66] Copyright©2021, The Royal Society of Chemistry. (b) SEM image of MXene/CNT nanofiber without any agglomeration.[67] (c) Mechanical toughness of MXene/CNT wet-spun fiber.[67] (d) Under stress conditions, CNT stretched, which ensured the mechanical toughness of the fiber. Reproduced with permission (b–d).[67] Copyright©2022, Elsevier.

Centrifugation was carried out repeatedly to concentrate (25 mg ml^{-1}) the MXene nanosheets, resulting in a liquid crystalline phase. For this high concentration, MXene dispersion possessed a viscosity of 3.87×10^3 Pa s without any aggregation.

Moreover, the shear stress gradually increased after a certain time, indicating the uniform orientation of MXene nanosheets. The as-prepared LC MXene dispersion was extruded into a coagulation bath of NH_4^+ ions and then washed with water to obtain the continuous pure MXene fiber. The prepared fiber showed a highly compact structure. Furthermore, the pure MXene fiber showed an ultrahigh electrical conductivity of 7713 S cm^{-1}, which is able to transmit signals from mobile phones.

In another study, it has been seen that to fabricate MXene fibers, MXene nanosheets were mixed with glutaraldehyde solution to induce liquid–crystalline properties.[71] High-concentrated, 30 mg ml^{-1}, spinning solution exhibited a viscosity of 4.1 kPa s, suggesting good spinning properties. This highly concentrated MXene spinning solution was extruded into a coagulation bath which contained ammonium chloride, ammonium hydroxide solution, and deionized water. Then the fiber was transferred into a PVA solution followed by washing with deionized water to obtain the MXene (MGP) fibers.

The obtained MGP fibers were further transferred into a polymer tube for thermal drawing. Thus, the obtained fiber showed a high mechanical strength of 585.5 MPa and a high electrical conductivity of about 8802.4 S cm^{-1}.

Biscrolling

The biscrolling technique involves the guest–host concept to fabricate hybrid yarn by using twist-based spinning.[72] Nowadays, this unique technique is used to fabricate MXene-based yarn. Regarding the fabrication of MXene-based yarn, MXenes serves the purposes of guest materials, and carbon nanotube (CNT) is used as the host material. This technique may allow high electrochemical performance, electrical conductivity, and mechanical properties. For example, Yu *et al.* fabricated MXene/CNT fiber by biscrolling technique.[73] The $Ti_3C_2T_x$-MXene nanomaterials were dispersed in water/DMF solution followed by drop-casting on CNT scaffold using a pipette. Then MXene/CNT thin film was scrolled into a helical fiber. This process allowed higher loading of $Ti_3C_2T_x$-MXene (95%) as the guest materials into the corridor of the CNT scaffold. In such a guest–host hybrid structure, CNT served the purpose of mechanical robustness and higher electrical conductivity. As a result, the fiber material can be used in different forms, such as knitted and woven into a glove, or wound around a glass rod. The fabricated yarn exhibited higher mechanical strength (38.4 MPa), higher electrical conductivity (270 S m^{-1}), and excellent volumetric capacitance (22 F cm^{-3}). This proves that the biscrolling technique is useful for fabricating MXene-based yarn for the production of smart textiles. Wang *et al.* also followed the biscrolling strategy to prepare $Ti_3C_2T_x$-MXene/CNT yarn, referred to as BMX yarn.[74] They drop casted MXene dispersion on CNT-stacked nanosheets. Then MXene/CNT hybrid was twisted using 2000 turns per m to fabricate the yarn. In this technique, the guest materials, MXene, can be confined within the corridor of the host materials, CNT, creating a porous structure. This pore volume and hydrophilic nature of MXene nanosheets allow fast electrolyte ion transportation, which improves the electrochemical performance. The biscrolling technique is very useful for producing flexible, high-strength conductive yarn that may facilitate the fabrication of smart wearable garments for multiple applications. However, the main disadvantage of this technique is limited to CNT as the host material.[23]

Although the coating, electrospinning, wet-spinning, and biscrolling techniques are extensively used for fabricating MXene-based textronics, these fabrication approaches exhibit certain flaws. For instance, regarding the coating process, uneven formation of MXene nanosheets may occur on the surface of textile substrates if MXene dispersion and concentration are not maintained properly. Table 1 represents a comprehensive overview of the advantages and disadvantages of different approaches.

Table 1 Advantages and disadvantages of different approaches to fabricating MXene-based textronics

Fabrication method	Advantages	Disadvantages	Ref.
Coating	• Simple and fast fabrication process • Lower cost • Large scale production	• Uneven thickness of electroactive materials • Careful selection of a concentration of electroactive materials • Limited to surface coverage	20
Biscrolling	• No need for a binder • Accessible to high loading of guest materials • Highly porous yarn can be prepared	• The host material is limited to CNT • Limited length of yarn	123
Wet spinning	• Continuous length of the fiber • Scalable production	• Careful selection of coagulant solvent, rheology of spinning solutions, and spinning setup	124
Electrospinning	• High surface area to volume ratio of the nanoscale fiber • Various composite nanofibers can be produced	• Difficult to fabricate electroactive materials • Tends to agglomeration • High voltage requirements	125

Affecting factors for enhancing the functional properties

Fiber type. Fiber type plays an important role because it influences the final properties of MXene-based textronics. Cotton, polyester, Kevlar, wool, silk, *etc.* are distinct in terms of their properties. For instance, Kevlar, aramid or basalt fibers are stronger than cotton or wool fibers. Therefore, such high-strength fibers should be used where higher strength is needed, for example, body armor for soldiers. It has been seen that the MXene-modified basalt fiber-reinforced polymer matrix showed an ultrahigh strength, 530.1 MPa of flexural strength and 26.7 GPa of flexural modulus.[75]

In addition, aramid nanofiber-reinforced $Ti_3C_2T_x$/silver nanowire composites showed outstanding mechanical properties with a tensile strength of 235.9 MPa and a fracture strain of 24.8%.[76] The high mechanical strength of aramid nanofiber can be ascribed to hydrogen bonding, π–π stacking, and van der Waals forces between the amide linkage of aramid fibers.[77] On the other hand, MXene/waterborne polyurethane (WPU) deposited nonwoven fabric, made from polyester fiber, showed a tensile strength of about 25.78 MPa.[78] This lower mechanical strength may arise due to the less polymer linkage in the polyester fiber than the aramid fiber. In addition, if MXene-based textronics are needed to be used as a flexible, wearable sensor or thermal device, then fiber elasticity is needed for this purpose. Regarding this lycra fiber (spandex yarn) can be used because it possesses high elastic properties.[79] For instance, MXene-modified cotton/spandex yarn (MCSY) showed excellent recoverability with up to 100% stretching.[31] In addition, at 20% strain, the stretch recoverability after 20, 80, and 100 repeated tensile cycles was almost identical. Fig. 4(a) shows the stretching behavior of the yarn. Such MXene-coated yarn showed a wide sensing performance when attached to the human wrist and back neck, as shown in Fig. 4(b).

Fabric structure. Not only the use of fiber but also the fabric structure plays a vital role in enhancing the functional properties of MXene-based textronics. Especially, air permeability, the main parameter of comfortability, and conductivity largely depend on the fabric structure because fabric structure exhibits gaps between the adjacent yarns. The smaller gaps ensure the more compact and uniform coating of MXene nanosheets, whereas the larger pores allow to pass out more MXene molecules. This directly affects the conductivity. Moreover, the production cost may also increase because the excess amount of MXene nanomaterials is needed to deposit on the larger pores-sized fabric compared to the smaller ones. The pore size of the fabric depends on the type of fabric structure. For instance, woven fabrics have a more compact structure than knitted fabrics, which may allow the uniform deposition of MXene nanomaterials. In addition, it is also possible to produce various types of woven fabrics (*e.g.* plain weave, satin, weave, twill weave, diamond, *etc.*) and knitted fabrics (*e.g.* single jersey and double jersey, plated patterns, *etc.*), which also possess different pore sizes according to their design.

It has been seen in a study that the load capacity of MXene nanomaterials on three different weave structures, plain, twill,

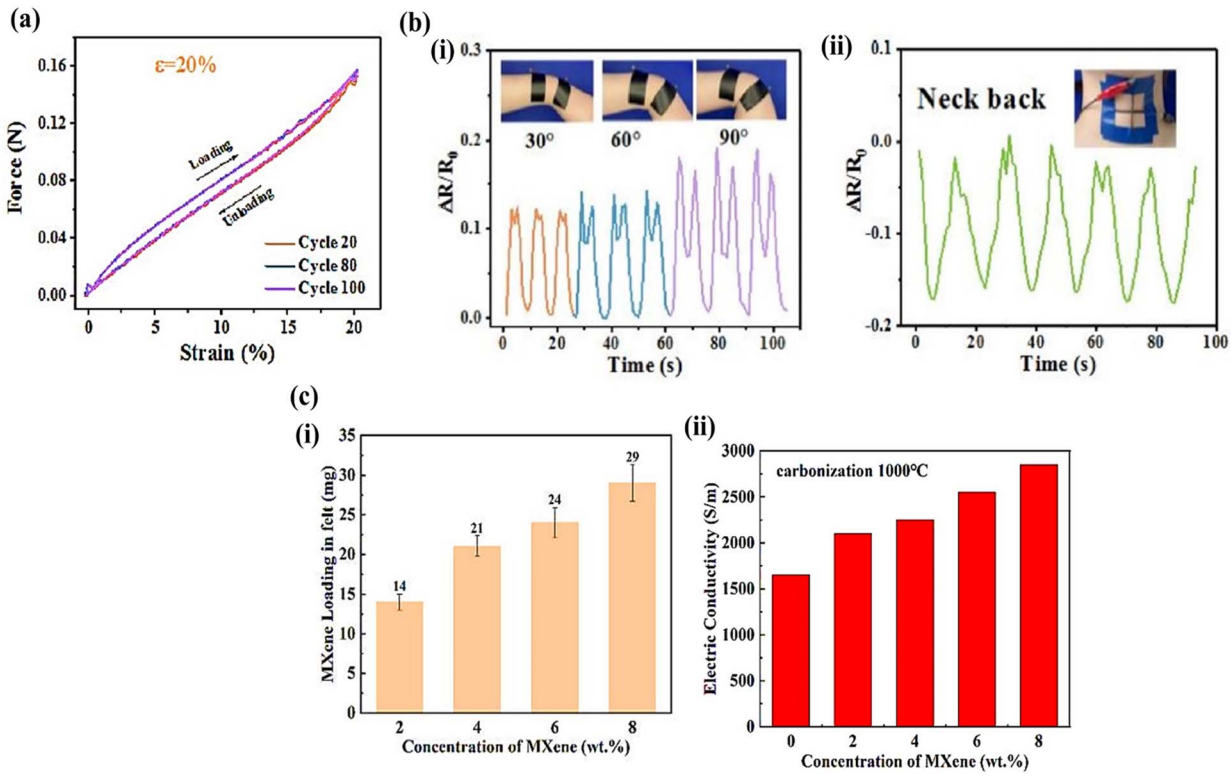

Fig. 4 (a) Identical force–strain curve of MXene/cotton/spandex yarn.[31] (b) Sensing application of MXene/cotton/spandex yarn when attached to wrist (i) and neck back (ii). Reproduced with permission (a and b).[31] Copyright©2023, American Chemical Society. (c) Increase of MXene loading and electrical conductivity with the increase of MXene concentration.[81]

and satin, of cotton fabrics was investigated to understand the photothermal and sensing performances.[80] After dip coating the fabrics into 5 mg ml^{-1} MXene solutions, three different levels of MXene contents were achieved, 0.175 mg cm^{-2}, 0.228 mg cm^{-2}, and 0.297 mg cm^{-2} for plain weave, twill weave, and satin weave respectively. That is why the satin fabric showed the highest conductivity for satin weave. The highest MXene content for satin fabric can be ascribed to its fewer interweaving points, higher density, and thicker structure than the plain and twill weave. As a result, MXene-decorated satin fabric showed excellent photothermal properties with an ultrahigh temperature of 251.7 °C as well as a wide pressure range of 20 kPa as the pressure sensor.

Besides the traditional two-dimensional (2D) fabric structures (*e.g.*, knitted and woven), three-dimensional (3D) fabric structures highly influence the functional properties of MXene-based textronics as, unlike the 2D fabric structure, the 3D structured fabric possesses a higher surface area increasing the MXene loading percentage on the fabric surface. For instance, Fan *et al.* prepared 3D denim fiber from waste jeans, which was immersed in MXene solution to form a conductive layer.[81] As the 3D structure has additional fiber direction (*Z* direction) along with *X* and *Y* directions, the 3D denim fiber provides a higher contact area, increasing the MXene loading and electrical conductivity, as shown in Fig. 4(c). Therefore, the fabricated conductive 3D denim fiber showed a superior specific capacitance of 1748.5 mF cm^{-2} and a remarkable stability of more than 94% after 15 000 charge/discharge cycles.

Surface modification by carefully chosen materials. MXene-based textiles can show high electrical conductivity, which facilitates the preparation of wearable electronics. As this wearable electronic device is attached to the human skin, it should be carefully noticed on some special properties, such as air-permeability, antibacterials, flame retardancy, wound-healing, sensitivity, and so on. These properties can be improved by introducing additional materials with MXene-based textiles. The hydrophilic properties and the easy-care pre-treatment facilities of the textile substrates make it easy to modify the MXene-based textronics to introduce multi-functionality. For instance, to increase the thermal conductivity or EMI shielding properties, the addition of conductive fillers with organic or inorganic polymers is considered the most efficient way.[82] Qian *et al.* fabricated $Ti_3C_2T_x$/hexagonal boron nitride (h-BN) composite film, where the conductive fillers, $Ti_3C_2T_x$ and h-BN, were dispersed into cellulose nanofiber (CNF) suspension,[83] where CNF acted as the binder. The negatively charged $Ti_3C_2T_x$ and CNF were coulombic assembled with positively charged h-BN during the fabrication process, causing the tightly packed film, zigzag fracture structure composite film, as in Fig. 5(a). Moreover, due to the use of h-BN nanomaterial with $Ti_3C_2T_x$, the thermal conductivity was enhanced to 8.03 W mK^{-1} compared to the $Ti_3C_2T_x$/CNF film (7.01 W mK^{-1}). In addition, using h-BN conductive nanofiller and increasing the MXene amount caused the enhancement of electrical conductivity from 4.96 S cm^{-1} to 57.67 S cm^{-1}. Besides the use of additional conductive fillers, fabricating porous, spongy 3D

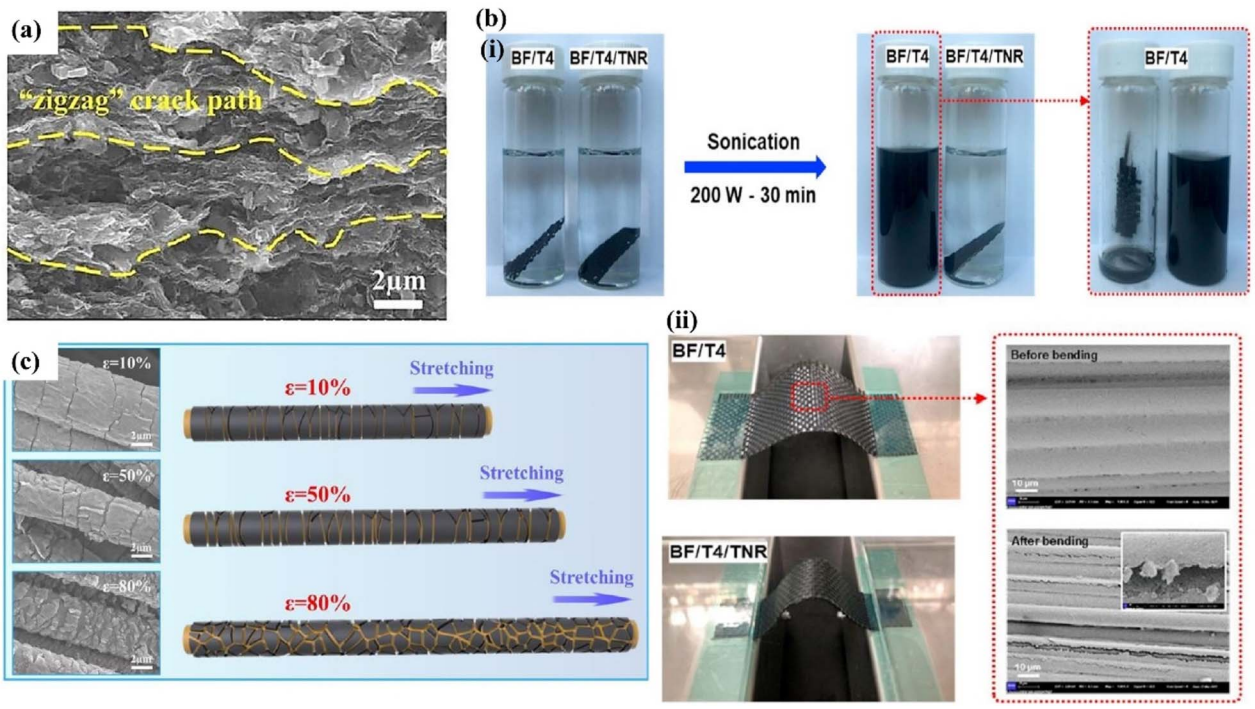

Fig. 5 (a) SEM image of fractured surface of $Ti_3C_2T_x$/h-BN hybrid film. Reproduced with permission.[83] Copyright©2022, Elsevier. (b) Photograph of 4 mg cm^{-2} $Ti_3C_2T_x$-decorated basalt fabric (BF/T4) and 4 mg cm^{-2} $Ti_3C_2T_x$/natural rubber-decorated basalt fabric with (BF/T4/TNR) before and after ultrasonication (ii) and bending treatment of BF/T4 and BF/T4/TNR. Reproduced with permission.[86] Copyright©2021, Elsevier. (c) SEM image of the cracked surface of MXene/cellulose nanocrystal-modified thermoplastic polyurethane (TPU) non-woven fabric. Reproduced with permission.[87] Copyright©2020, The Royal Society of Chemistry.

networks also enhances the electrical pathways. It has been seen that ferromagnetic $Fe_xCo_{1-x}P$ porous spongy nanostructure (SNS) on the surface of woven Kevlar fabric (WKF) provided the electrical pathways for enhanced charge transfer.[84] Moreover, MXene/PDMS dispersion was coated on this porous structure by spin coating. The $Fe_xCo_{1-x}P$ SNS held the MXene nanosheets, developing 3D MXene nanostructure. This porous interconnected 3D network resulted in high Joule heating (74 °C at 3 V), which helped to maintain body warmth. The porous composite also exhibited high impact resistance at 131.4% for use as a smart body armor.

Although MXene has been widely used in wearable electronics due to its remarkable properties, fabricating MXene-based smart textiles that overcome the MXene oxidation problem is still challenging. Creating a hydrophobic surface may solve this issue. The polydimethylsiloxane (PDMS) layer, for example, was deposited on the MXene-coated textile surface by a simple dipping and drying process.[85] This PDMS layer not only created superhydrophobicity but also protected MXenes from oxidation without sacrificing breathability and strength properties. Due to creating a hydrophobic surface on the MXene-coated textile surface, MXene nanosheets do not come into contact with moisture content. Therefore, it is protected from oxidation. Furthermore, the amount of MXene nanomaterials may create cracks surface due to the rigid conductive layer during the bending of MXen-modified fabric surfaces, especially on synthetic polymeric fiber (SPF), like Kevlar, aramid, basalt, and polyester.

Unlike cotton, silk, or wool fabric, these fibers may not easily form bonds with the surface functional groups of MXene nanomaterials. Plasma treatment is now widely used to create functional groups on the surface of SPF to bind the MXenes. However, the bonding structure may loosen, if the MXene-modified SPF is introduced to the harsh environment. For instance, ultrasonicating the $Ti_3C_2T_x$-modified basalt fabric caused the detachment of Ti_2CT_x from the fabric.[86] In addition, bending the $Ti_3C_2T_x$/basalt fabric created the crack surface. To solve this problem, $Ti_3C_2T_x$ was dispersed with natural rubber content and coated on the $Ti_3C_2T_x$/basalt fabric. Fig. 5(b) shows the ultrasonication and bending treatment of such fabric. The modified fabric in this way showed superior electromagnetic shielding, much better than the pure MXene modified fabric. Generally, to obtain high-performance EMI shielding properties using MXene nanomaterials, it should be ensured the uniform coating of MXene nanosheets because MXene nanosheets can consume electromagnetic waves. Therefore, any disruption of conductivity may deteriorate the EMI performance.

However, to fabricate the MXene/textile-based wearable pressure/strain sensor device, increasing the resistivity plays a crucial role because the pressure sensitivity is defined by the gauge factor, which can be calculated by this rule: $GF = (\Delta R/R_0)/\varepsilon$, ε refers to the applied tensile strain, $\Delta R = R - R_0$, where R is

Table 2 Influence of using different materials on the functional properties of MXene-based textronics

Textronic architecture	Surface modifier (S.M.)	Purpose of using S.M.	Property enhancement	Ref.
$Ti_3C_2T_x$/h-BN	CNF	Binder of conductive fillers	Tensile strength, thermal conductivity	83
Spongy $Fe_xCo_{1x}P$/WKF/MXene	Spongy $Fe_xCo_{1-x}P$	Increasing the conductive pathway, bind MXene nanosheets to solve the aggregation problem	Conductivity, joule heating, impact resistance	84
MXene–PPy textiles	Polypyrrole	Protective layer to avoid the oxidation of MXene nanosheets	Capacitive performance	126
PPy/MXene decorated PET textiles	Polypyrrole, silicone	Formation of highly conductive path, stability, and prevents MXene oxidation problem	Water resistance, electrical conductivity, EMI shielding performance, Joule heating performance	22
MXene/CNC coated TPU fabric	CNC	Achieving stable and homogenous MXene dispersion with good strength and binding properties	Enhance the sensing properties	87
	PDA	Increasing the wettability of TPU NWF		
AgNW/MXene/PET textiles	PDA	Enahnce the bonding strength	EMI shielding and sensing performance	127
	AgNW	Forming 3D conductive network		
AgNW@MXene coated PET textiles	NaOH	Improve the surface activity of PET textiles	Improve antibacterials, flame retardant, EMI-shielding, electrothermal and photothermal performances	128
	PVP	Enhance the bonding strength between PET and AgNW along with MXene		
	AgNW	Enhance the conductivity		

resistance after applying pressure and R_0 is the initial resistance. When external pressure is applied, the conductive path is disrupted, causing the enhancement of sensitivity. Creating micro-crack structures within the MXene-modified fabric may enhance the sensitivity as the crack surface hinders electron transportation. Li *et al.* fabricated MXene/cellulose nanocrystal-modified thermoplastic polyurethane (TPU) non-woven fabric, where special pre-stretching treatment was applied to the conductive non-woven fabric (NWF), as shown in Fig. 5(c).[87] From this figure, it has been seen that increasing the tensile strain created a more open structure in the fabric, indicating a sharp increase in sensitivity. For these reasons, the materials and the fabrication process should be carefully chosen accordingly during the fabrication of MXene-based textronics. Table 2 represents an overview of how different types of materials affect the end uses of MXene-based textronics.

MXene size. MXenes size has a substantial effect on the functional properties of MXene-based textronics. The etching methods of $Ti_3C_2T_x$-MXene endow the numerous functional groups on the MXene surface and it also affects the MXene flake size.[88] For instance, reducing the amount of HF solution by using the combination of HCl, water, and HF in a 6 : 3 : 1 volumetric ratio during the preparation of Ti_3C_2 MXene resulted in a larger size of MXene nanomaterials.[89] Moreover, the combination of LiF and HCl instead of HF solution during the etching of MAX precursors caused the larger size MXene flakes.[90] Besides the etching methods, post-treatment of MXene nanosheets also affected the MXene size. For instance, Maleski *et al.* investigated the sonication effect on MXene lateral sizes, which causes the alteration of electrical conductivity.[91]

The average size of $Ti_3C_2T_x$ flakes was 4.4 ± 1.5 μm without sonication, however, the size reduced to about 0.13 ± 0.06 μm after probe sonication at 250 W. The highest average size of MXene flakes showed a conductivity of approximately 5000 S cm^{-1}, whereas the smallest size exhibited a conductivity of about 1000 S cm^{-1}. The reduction of conductivity with the reduction of MXene flake sizes may be ascribed to the more compact structure, resulting in interfacial resistance which causes the lower conductivity. Therefore, it has been seen that the conductivity of MXene nanomaterials largely depends on

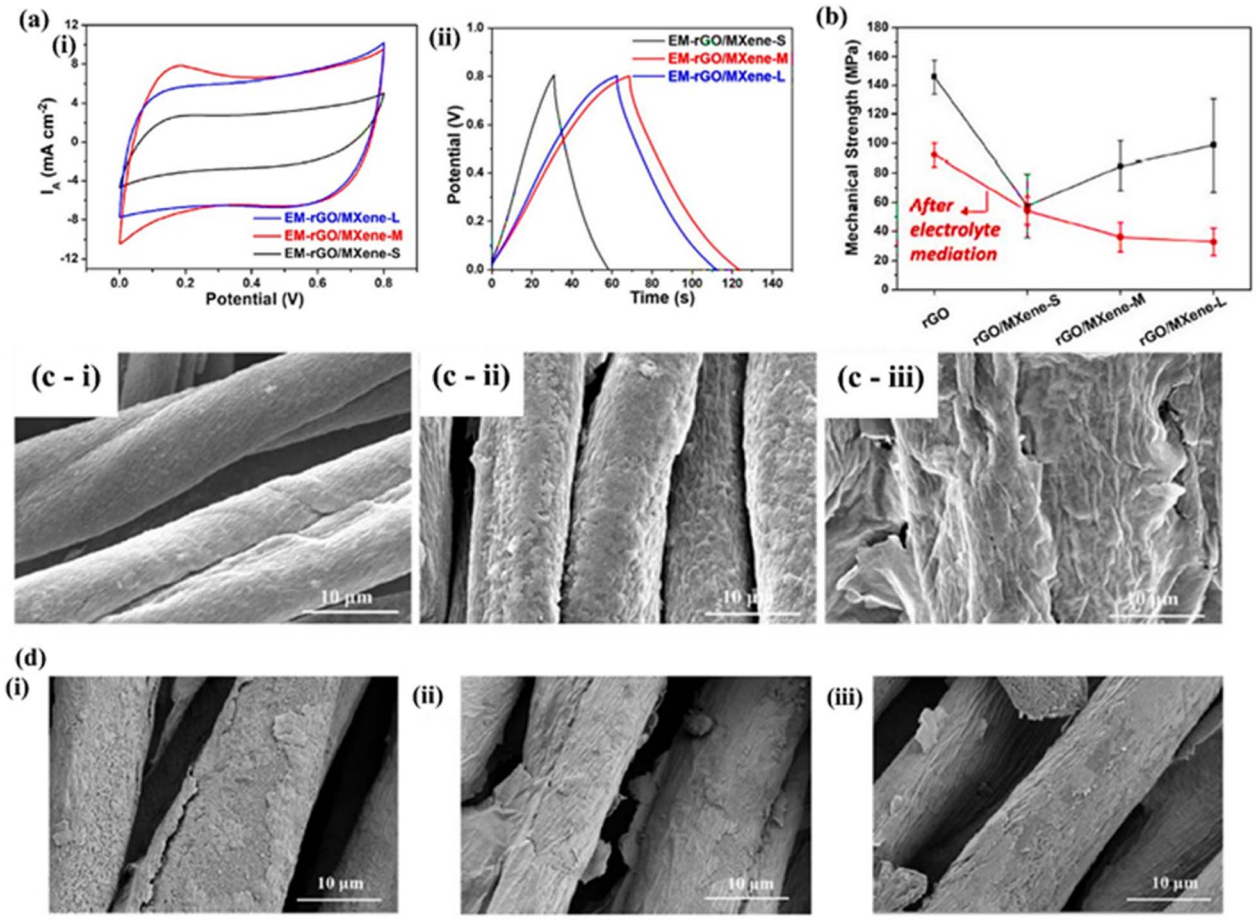

Fig. 6 (a) Cyclic voltammetry (i) and galvanostatic charge–discharge (ii) curves of electrolyte-mediated rGO/MXene fibers with large, medium, and small size MXene.[92] (b) Mechanical strength of pure rGO and rGO/MXene fibers with small, medium, and large size MXene before and after electrolyte mediation. Reproduced with permission (a and b).[92] Copyright©2020, American Chemical Society. (c) MXene-modified fabric with small size MXene (i), a combination of small/large size MXene (ii), and large size MXene (iii).[94] (d) SEM image of MXene-modified fabric with small size MXene (i), a combination of small/large size MXene (ii), and large size MXene (iii) after washing. Reproduced with permission (c and d).[94] Copyright©2022, Elsevier.

MXene sizes, which can affect the functional properties of MXene-based textronics. He *et al.* explored the electrochemical performance of $Ti_3C_2T_x$-MXene/rGO fiber on the basis of different sizes of Mxenes.[92] They found that the MXene/rGo fiber, prepared by large-size MXene (6 μm), showed higher conductivity than the fiber fabricated by medium (2 μm) and small-size MXene (700 nm). Due to this superior conductivity, large-size and medium-size MXene caused better electrochemical performance than small-size MXene, as shown in Fig. 6 (a). However, from Fig. 6(b), it has been seen that the mechanical strength declined for large-size and medium-size MXene nanomaterials than the small-size MXenes after electrolyte mediation, which was ascribed to the reduction of interfacial interaction between MXene and rGO. Regarding supercapacitor applications, large-size MXene nanomaterials may ensure sufficient transportation pathways for electrolyte ions. Therefore, MXene nanoflakes with more open space are suitable for wearable supercapacitor applications. However, for wearable electronic devices, mechanical strength plays a crucial role, because it has undergone many deformations when worn on the human body. Therefore, optimizing the MXene sizes without compromising the strength is very necessary. Before considering this issue, the following effects of MXene nanosheets should be carefully observed: (1) MXene nanoflakes with smaller sizes show lower conductivity, however, it introduce defects on the MXene surface, causing the enhancement of electroactive sites that aid in increasing the capacitance;[93] (2) large MXene size enables the electrolyte ion transportation, although, it may reduce the strength due to lack of interfacial interaction. Considering the conductivity, wash fastness, and mechanical strength Zhang *et al.* formulated that the combination of small/large MXene coating on cotton fabric shows better electromagnetic shielding properties than the large and small MXene.[94] They concluded that small MXene covered the fiber surface due to its tiny size, while it did not allow the coverage of pores of the fabric. However, the large MXene covered the pore space, allowing a more conductive path, as shown in Fig. 6(c). After washing, the large MXene tended to fall off and small MXene remained on the surface of the fabric. Therefore, regarding the combination of small/large MXene, small MXene covered the fiber or yarn surface, while large MXene bridged the between the yarn, increasing the binding force. Fig. 6(d) shows the coating of three different sizes of MXene on the fabric surface after washing. The conductive effect and the functional properties of different sizes of MXene materials are shown in Table 3.

Applications of MXene-based textronics

Wearable supercapacitor

Nowadays, to tackle the high energy consumption, the demand for alternative energy sources has been escalating. Regarding this, the flexible wearable supercapacitor is gaining popularity in day-to-day life because supercapacitors exhibit high power density, less charge–discharge time, and longer life cycles than conventional batteries and capacitors.[95,96] In addition, the usability of flexible wearable supercapacitors can be ensured by analyzing the electrochemical performance, such as power density, energy density, capacitance (areal or gravimetric), and

Table 3 Effect of MXene size on conductivity, strength, and performance of MXene-based textronics

MXene textronics	MXene size	Conductivity	Strength	Performance	Ref.
—	4.4 ± 1.50 μm	~5000 S cm^{-1}	Not reported	Capacitance: 270 F g^{-1} at 2 mV s^{-1}	91
	0.13 ± 0.06 μm	~1000 S cm^{-1}		Capacitance: 260 F g^{-1} at 2 mV s^{-1}	
MXene/carbon nanofiber (CNF) film	0.7–0.8 μm	Not reported	Not reported	Capacitance: ~113 F g^{-1} at 5 mV s^{-1}	129
	2–3 μm			Capacitance: ~113 F g^{-1} at 5 mV s^{-1}	
	6–8 μm			Capacitance: 106 F g^{-1} at 5 mV s^{-1}	
rGO/MXene fiber	6 μm	627.6 ± 68.5 S cm^{-1} After electrolyte filtration: 292.8 ± 5.8 S cm^{-1}	98.8 ± 31.9 MPa After electrolyte filtration: almost 33 MPa	Not reported	92
	2 μm	Almost 482 S cm^{-1} After electrolyte filtration: almost 250 S cm^{-1}	Approximately 87 MPa After electrolyte filtration: almost 38 MPa	Not reported	
	700 nm	Almost 165 S cm^{-1} After electrolyte filtration: almost 55 S cm^{-1}	Almost 60 MPa After electrolyte filtration: almost 57 MPa	Not reported	
PVA/MXene film	10 μm	~6240 S cm^{-1}	280 MPa	Capacitance: 364 F g^{-1}	130
MXene coated cotton yarn (MY)	927 nm (L)	50.8 S cm^{-1}	Not reported	Wash fastness: SL-MY > L-MY > S-MY	94
	284 nm (S)	20.4 S cm^{-1}			
	Combination of 927 & 284 (S/L)	49.3 S cm^{-1}			
MXene coated cotton fabric (MF)	927 nm (L)	891 S m^{-1}	Not reported	SE before washing: LMF > SLMF > SMF & SE after washing: SLMF > LMF > SMF	94
	284 nm (S)	2020 S m^{-1}			
	Combination of 927 nm & 284 nm (S/L)	2245 S m^{-1}			

electrochemical impedance system, under bending, folding, or torsion conditions. In terms of wearability, textile-based materials such as fiber, yarn, or fabric, have been considered most due to their lightweight, high bending capacity, and superior comfortability.[97] Furthermore, there are enormous opportunities for surface modification of textile materials to deposit the electroactive materials, which makes it suitable for wearable supercapacitor applications. Among various conductive materials, MXene has been recently used extensively for the fabrication of textile-based wearable supercapacitor devices.[15,98] There are various ways to load the MXene on the textile's surface, such as coating, spraying, wet spinning, and many others. After modifying the textile's surface with MXene materials, the electrochemical performance of textile-based supercapacitor devices has been enhanced significantly. For instance, Shao *et al.* developed a new method of nanofiber-coated yarn *via* electrospinning.[58] They electrospun MXene polymer composite nanofiber on polyester (PET) yarn to obtain MXene nanofiber coated yarn electrode to use as a wearable supercapacitor. The prepared all-solid-state supercapacitor with the yarn electrode showed an areal capacitance of 18.39 mF cm^{-2} at 5 mV s^{-1}. In addition, the supercapacitor device showed 98.2% capacitance retention after 6000 cycles. In another study, it has been found that combined technique of electrospinning and wet spinning were used for producing MXene/nylon nanoyarn to use as a energy storage device.[99] Such yarn electrodes exhibited a high specific capacitance of 440 F cm^{-3} at 5 mV s^{-1} in $LiClO_4$ electrolyte solution. Besides the spinning process, the layer-by-layer (LBL) assembly technique is also used for preparing wearable supercapacitor devices. LBL is a multilayer fabrication technique of thin film. Regarding this technique, oppositely charged materials are deposited alternately on a solid substrate multiple times.[100] Yun *et al.* prepared wire-shaped supercapacitors (WSCs) by the LBL method, where positively charged reduced graphene oxide functionalized with poly-(diallyldimethylammonium chloride) and negatively charged $Ti_3C_2T_x$ MXene were alternately deposited on activated carbon yarns.[101] The LBL-coated activated yarn (LACY) with 40-layer pairs (LP) showed rectangular cyclic voltammetry (CV) curves for different scan rates, as shown in Fig. 7(a). These prove a good capacitive behavior of WSCs. Furthermore, the WSCs also showed no significant change in CV curves under different bending conditions, as illustrated in Fig. 7(b). Besides the electrospinning process, to fabricate the MXene integrated yarn electrode, coating techniques, such as dip coating, *in situ* polymerization, or drop-casting, are also widely used, which are considered the easiest methods. For instance, Yang *et al.* dipped cotton yarn into a mixture of pyrrole and MXene solution and then soaked it into 1 wt% sodium anthraquinone sulfonate ($C_{14}H_7NaO_5S$) and a 4 wt% ammonium persulphate ($(NH_4)_2S_2O_8$) to initiate the polymerization process.[32] The areal capacitance of PPy/MXene@cotton electrode reached to 455.9 mF cm^{-2} at scan rate of 0.9 mA cm^{-2}.

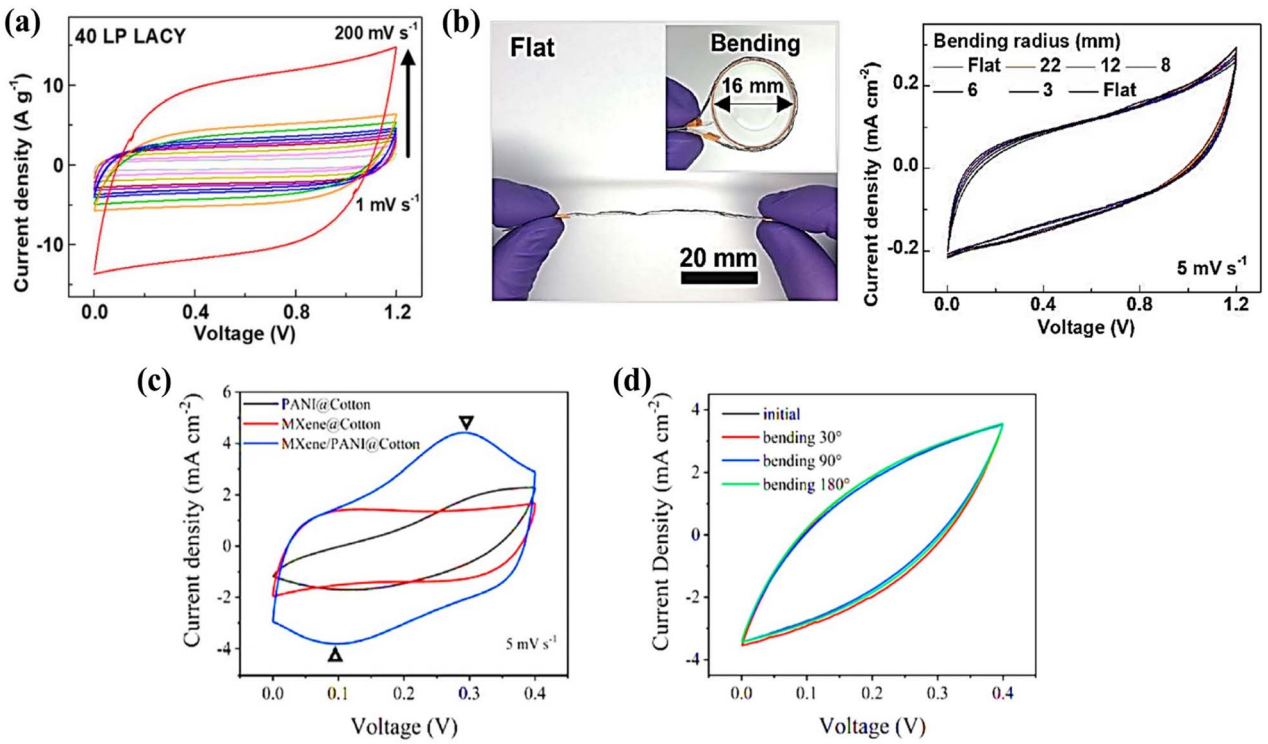

Fig. 7 (a) Cyclic voltammetry curve of carbon yarns coated with rGO and MXene.[101] (b) Flat and bending condition of rGo/MXene coated carbon yarns (i) and cyclic voltammetry curves of MXene modified carbon yarns under different bending stages, proving its superior capacitive performance (ii). Reproduced with permission (a and b).[101] Copyright©2021, American Chemical Society. (c) Cyclic voltammetry curve of PANI/cotton, MXene/cotton, and MXene/PANI cotton.[102] (d) Identical cyclic voltammetry curves of symmetry supercapacitor devices prepared by MXene/PANI/cotton electrode at different bending angles. Reproduced with permission (c and d).[102] Copyright©2023, Elsevier.

Besides the fabrication of yarn-based electrodes for supercapacitor applications, 2D-like fabrics, knitted, woven, or nonwoven, are also used for supercapacitor applications. Ye *et al.* took the advantage of *in situ* polymerization technique to modify the knitted cotton fabric with polyaniline.[102] Then PANI/cotton fabric was dipped into MXene solution to get MXene/PANI@cotton electrode. From Fig. 7(c), it has been seen that MXene/PANI@cotton electrode showed the highest CV curve area than MXene/cotton and PANI/cotton electrodes, indicating the highest capacitance behavior. This highest capacitance is mainly derived from the coating of double-conductive materials on the fabric. Furthermore, to understand the real-life applications, a sandwich-like supercapacitor (SC) device was fabricated by using MXene/PANI@cotton electrode, poly(vinyl alcohol) (PVA)–H_2SO_4 gel as electrolyte and separator. The SC device maintained 58.8% capacitance retention after 1000 cycles. Moreover, the CV curves of the SC device at different angles, as shown in Fig. 7(d), did not show any significant change, indicating that the SC device maintained excellent capacitance under bending conditions. Li *et al.* fabricated MXene-coated cotton fabric (MCF) to use for a personal body thermal management system, where a supercapacitor device made with MXene-coated cotton electrode was used as the power source.[103] For MXene coating, the pretreated cotton fabric was dipped into 4 mg l^{-1} MXene solution for 5 minutes. The MCF electrode showed the highest capacitance of 208 mF cm^{-2} at the scan rate of 5 mV s^{-1}. For real-life applications, MCF electrodes were used to prepare a symmetric device, where 3 devices were connected in series connection by using the bipolar concept. In addition, 4 bipolar were also connected in parallel combination. Moreover, the joining of the MCF electrode and supercapacitor device on the elbow demonstrated the feasibility of real-life applications.

To understand the real-world applications of supercapacitors, it is necessary to prepare supercapacitor devices, symmetric or asymmetric, using electrode materials. The electrochemical performance of the electrodes can only show the potential applications. However, the specific capacitance, energy density, and power density measurements of supercapacitor devices are necessary to understand real-life applications. Table 4 represents an overview of different fabrication strategies to fabricate electrode materials using MXene and textile substrates, specific capacitance, and their real-world applications.

Wearable thermal device

Textronics are widely used for healthcare systems to diagnose diseases .[104–106] In addition, wearable textile devices are not only used for diagnosing but also are extensively used for therapeutic applications.[107] Regarding therapeutic applications, 2D $Ti_3C_2T_x$-MXene materials are extensively used as MXene materials possess excellent photothermal and electrothermal properties. MXene has localized surface plasmon resonance (LSPR) properties for which MXene materials show strong absorption in the solar spectrum.[108] Therefore, MXene-modified yarn or fabric is used for thermotherapy applications, such as wound healing, antibacterial, warm, protective fabric for cold environments, and so on. For example, Gong *et al.* fabricated $Ti_3C_2T_x$-MXene/polydopamine (PDA)/Ni^{2+} coated spandex yarn (MPNi@spandex) to use for wearable antibacterial therapy under near-infrared (NIR) irradiation.[109] The coated yarn exhibited excellent photothermal performance.

Fig. 8(a) demonstrates that the surface temperatures of the MXene-coated yarn were increased significantly with the increase of power density of NIR laser irradiation. Moreover, at the power density of 1.5 W cm^{-2}, the coated yarn showed excellent photothermal stability, as shown in Fig. 8(b). The excellent photothermal performance proved the potential application of $Ti_3C_2T_x$-MXene coated yarn for preparing wearable thermal devices. In addition, under the laser irradiation, MPNi@spandex yarn showed excellent antibacterial activity (more than 99.9%) than MXene (M@Spandex), MXene/PDA (MP@Spandex), and MXene/Ni^{2+} (MNi@Spandex) yarn, as demonstrated in Fig. 8(c). This excellent antibacterial property was attributed to the sharp edges, anionic, and hydrophilicity nature of MXene nanosheets at the yarn surface. Zhao *et al.* used a dip coating and drying process to convert non-woven fabric into $Ti_3C_2T_x$-MXene-loaded smart fabric.[110] The adsorption of MXene onto the fabric surface is mainly caused due to the strong hydrophilic properties of cellulosic fabric and the

Table 4 Real-life applications of supercapacitor devices prepared by MXene/textile-based composite electrode

Electrode	Fabrication method	Capacitance	Real-world applications	Ref.
MXene/cotton fabric	Dip coating	208 mF cm^{-2} at 5 mV s^{-1}	Body thermal management	103
PANI/MXene decorated PET fabric	Chemical polymerization and spray coating	647 mF cm^{-2} at 0.3 mA cm^{-2}	Powering a thermo-hygrometer	131
PPy/MXene/PEI-modified fabric	Chemical polymerization and dip coating	1295 mF cm^{-2} at 1 mA cm^{-2}	Powering digital watch	33
rGO/$Ti_3C_2T_x$ modified cotton fabric	Chemical reduction and spray coating	258 mF cm^{-2} at 5 mV s^{-1}	Powering a watch	132
$Ti_3C_2T_x$/carbon nanotube yarn	Biscrolling	3188 mF cm^{-2} at 2 mA cm^{-2}	Powering digital watch, digital timer	74
$Ti_3C_2T_x$/cotton yarn	Dip coating	3965 mF cm^{-2} at 2 mV s^{-1}	Capacitive pressure sensor	133
Ti_3C_2@PPy-CMC	Chemical polymerization and blending	100 F g^{-1} at 1 A g^{-1}	Glucose sensor	134
$Ti_3C_2T_x$/TPU/polypyrrole (PPy) fiber	Chemical polymerization and wet-spinning	41.2 F g^{-1} at 5 mV s^{-1}	Operating watch, electric meter	135

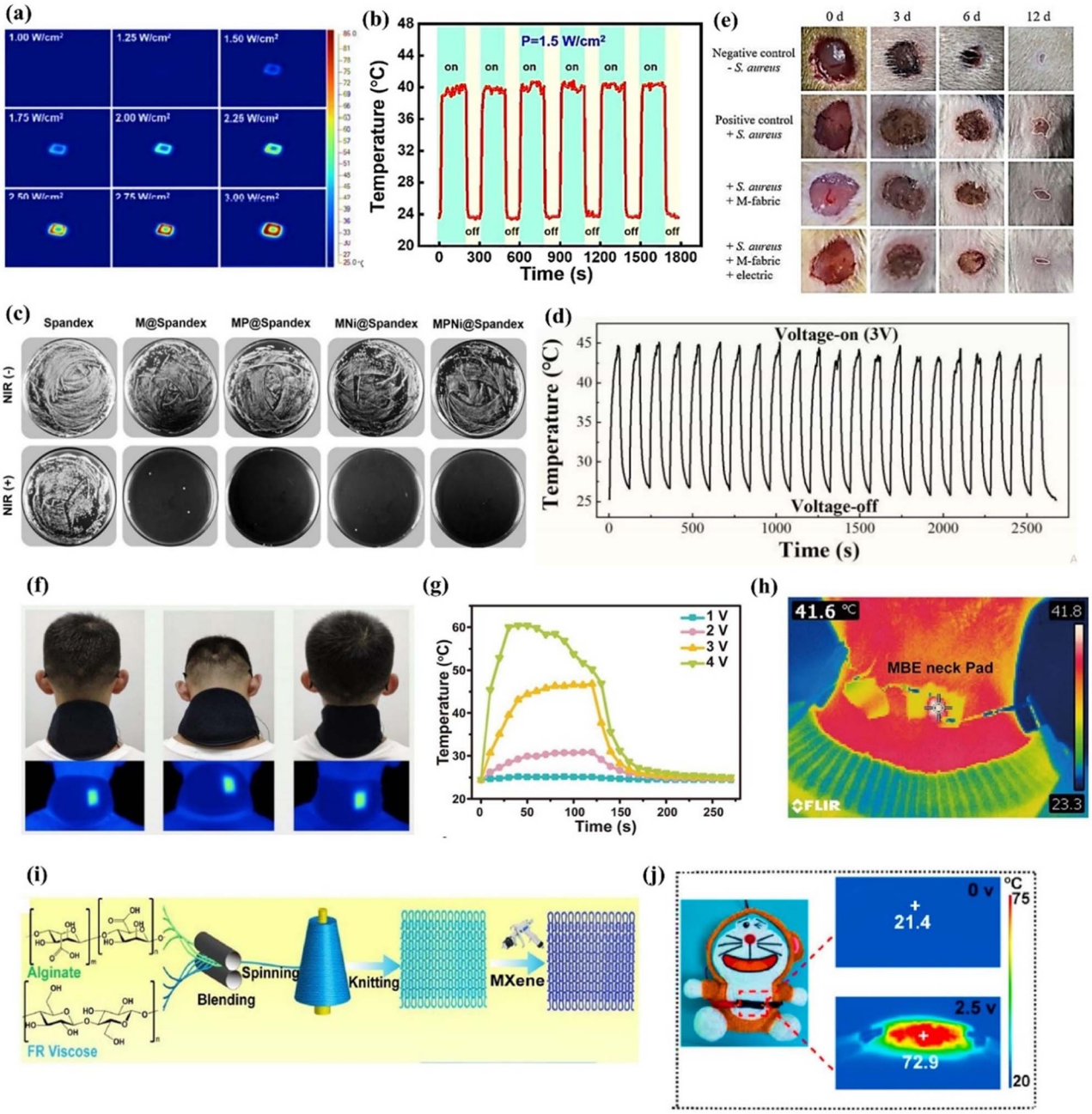

Fig. 8 (a) Increased surface temperature of MXene-modified spandex yarn with the increase of power density of NIR laser irradiation, indicating an excellent joule heating performance.[109] (b) Excellent photothermal stability of MXene-coated spandex yarn under the power density of 1.5 W cm^{-2}.[109] (c) Antibacterial properties of spandex yarn, MXene coated spandex, MXene/PDA coated spandex, MXene/Ni^{2+} coated spandex, and MXene/PDA/Ni^{2+} coated spandex yarn with NIR irradiation and without NIR irradiation. Reproduced with permission (a–c).[109] Copyright©2021, American Chemical Society. (d) Heat stability of MXene-coated non-woven fabric under a long time exposure.[110] (e) The differences in wound healing performances of only MXene-coated fabric and MXene-coated fabric under the applied electric voltage.[110] (f) The heating performance of the neck pad prepared by MXene-coated fabric under 3 V. Reproduced with permission (d–f).[110] Copyright©2020, American Chemical Society. (g) Electrothermal performance of MBE electrodes at input voltages of 1, 2, 3, and 4 V.[111] (h) The heating performance of the neck pad prepared by MBE electrodes at 3 V, demonstrating its practical application. Reproduced with permission (g and h).[111] Copyright©2022, American Chemical Society. (i) Fabrication process of MXene-coated alginate fiber and viscose fiber fabric.[112] (j) Thermal display of MXene-modified fabric when fixed on a toy. Reproduced with permission (i and j).[112] Copyright©2022, Elsevier.

presence of functional groups on MXene. The MXene-coated fabric (M-fabric) exhibited excellent heating durability, as shown in Fig. 8(d), which proved the potential thermotherapy application of M-fabric. For the application of bacterial-infected wound healing, Fig. 8(e) shows that the wounded areas of the SD rat were almost recovered while using M-fabric and electrical heating together. In addition, the neck guard pad made with M-fabric showed a stable heat generation under an applied voltage

Table 5 Overview of recent research progress of MXene-based textronics in thermotherapy applications

MXene-based textronics	Fabrication strategy	Real-life applications	Ref.
MXene-amoxicillin-PVA nanofibrous membrane	Electrospinning	Antibacterial therapy, wound healing	136
$Ti_3C_2T_x$/polydopamine/Ni^{2+} coated spandex yarn	Dipping and drying	Antibacterial therapy	109
$Ti_3C_2T_x$/Polypropylene (PP) fabric	Dipping and drying	Antibacterial therapy	137
$Ti_3C_2T_x$-coated grass-derived cellulose	Dip coating	Theranostic	111
AgNW–$Ti_3C_2T_x$ coated nono-woven fabric	Spray coating	Personal thermal management	138
$Ti_3C_2T_x$/polydopamine decorated cotton fabric	Vacuum-assisted filtration	Personal thermal management	139
$Ti_3C_2T_x$ coated fabric	Dip coating and drying	Antibacterial therapy, wound healing	110
MXene/PDMS/PDA/PU	Coating	Photothermal antibacterial activity	140
TPU/CS/MXene/AgNW film	Dip-coating and vacuum filtration	Photothermal therapy	141

of 3 V, as demonstrated in Fig. 8(f). Song *et al.* prepared MXene-based epidermal electrodes (MBE) by dip coating cellulose film into MXene dispersion.[111] Fig. 8(g) shows that the temperature of the MBE film electrode reached its maximum position at a certain applied voltage within a very short time. To understand the potential theranostic application, an MBE neck cushion was worn. Fig. 8(h) shows that heating occurred around the neck muscle at the applied voltage of 3 V. In another study, it has been seen that He *et al.* blended sodium alginate (SA) fibers and flame retardant viscose (FRV) fibers followed by spinning to obtain the blended yarn, as shown in Fig. 8(i).[112] The yarn was knitted to produce fabric by knitting machine. MXene solution was then sprayed onto the fabric. The MXene-modified fabric demonstrated a wide temperature range under different applied voltages, which proved the heating requirements of wearable thermal devices. In addition, to understand the human requirements of thermotherapy, the MXene-modified fabric was placed on a toy. After applying 2.5 voltage, the surface temperature reached 72.9 °C, as illustrated in Fig. 8(j). Table 5 illustrates the real-life applications of MXene-based textronics in thermotherapy.

Wearable sensor

At present, the demand for textile-based wearable electronic devices has been escalating. Due to the development of highly conductive MXene nanomaterials, a new form of smart textile that is a wearable sensor has been built recently, thanks to the discovery of MXene materials. For introducing MXene with traditional textiles, sensor performances, such as sensitivity, stability, and response time, are improved significantly.[20] In addition, lightweight, air permeability, high strength, and comfort are the ideal characteristics of textile-based wearable sensors. Furthermore, textile materials possess three different dimensional architectures which are one-dimension (*e.g.* fiber or yarn), two-dimensional (*e.g.* plane fabric), and three-dimensional (*e.g.* spacer fabric). Therefore, it is possible to develop new high-performance sensor devices by using textile substrates. In this section, the applications of MXene-based textile sensors in different fields are discussed elaborately.

Wearable strain sensor. MXene-based textile composite devices have high electrical conductivity, making them ideal candidates for wearable strain sensors. For instance, Zhang *et al.* prepared MXene-coated conductive fabric by spraying MXene inks (2 wt%, 4 wt%, and 6 wt%) on plain woven cotton fabric, followed by drying.[113] The obtained MXene/cotton fabric (M–CF) exhibited superior sensitivity at low bending strain, demonstrating its potential application in monitoring very small human activities.

Fig. 9(a) demonstrates that 2 wt% M–CF showed higher sensitivity than the other two samples 4 wt% M–CF and 6 wt% M–CF under the bending strain from 0 to 2.09%. Moreover, the developed sensor device easily detected pulse frequency, as shown in Fig. 9(b), demonstrating its potential application for human health monitoring. In another study, it has been seen that nylon fabric was dipped into MXene solution MXene solution for one hour to allow the uniform MXene coating, which was then treated with PDMS.

The as-prepared MXene/nylon sensor showed a gauge factor of 24.35 and 5.98 within the strain range of 20% in the axial and radial direction of nylon fabric, respectively.[114] Although textile substrates (fabric or yarn) exhibit excellent flexibility and stretchability for wearable sensor devices, some polymeric materials are also used as alternative flexible substrates to develop wearable sensors.

For example, thermoplastic polyurethane (TPU) was used as the flexible and stretchable substrate to develop an MXene-modified wearable sensor.[115] To increase the interfacial interaction between MXene and TPU, polyacrylonitrile (PAN) was introduced into the TPU substrate by electrospinning technique. The electrospun TPU/PAN substrate was then dipped into MXene inks to fabricate the MXene/TPU/PAN sensor device. The developed sensor exhibited a wide range of sensitivity, 7.01 and 9.69 under 1% and 80% strain respectively. Moreover, the strain sensor demonstrated a fast response (<140.6 ms) and a low limit of detection (<0.1%). This proved the potential application of MXene/TPU/PAN as the wearable sensor device.

Wearable pressure sensor. MXene-modified textile substrates are also extensively used to fabricate wearable pressure sensors. Regarding this sensor, sensitivity arises according to the change of conductivity, when the pressure sensor device is subjected to external pressure. Here, MXene acts as the conductive filler, which is stimulated with the applied pressure, causing the change of current. The sensitivity of the pressure sensor can be measured by this formula: $S = (\Delta I/I_0)/\Delta P$, where ΔI is the current change before and after the applied pressure on the devices, I_0 is the initial current when no pressure is

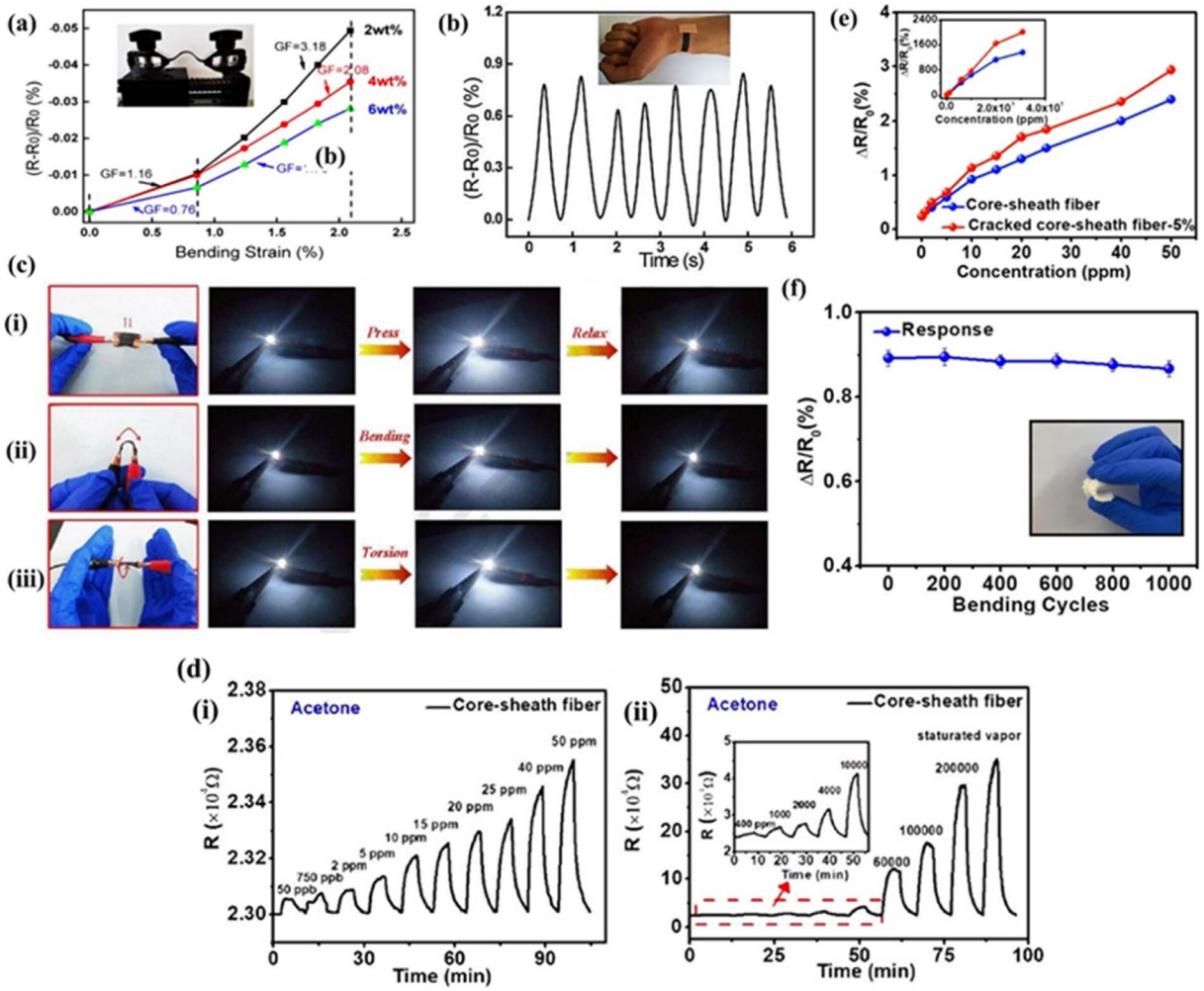

Fig. 9 (a) Strain sensing performance of MXene-coated cotton fabric under bending condition at different MXene loading%.[113] (b) Pulse frequency detection of MXene-coated cotton fabric. Reproduced with permission (a and b).[113] Copyright©2020, American Chemical Society. (c) LED light response of MXene/SiNPs modified fabric sensors under press (1), bending (2) and torsion (3) conditions. Reproduced with permission.[118] Copyright©2021, Elsevier. (d) Relative resistance change of MXene/PU core–sheath fiber regarding the acetone gas molecules detection ranging from 50 ppb to 50 ppm (1) and from 400 ppm to saturated vapor (2).[120] (e) Difference in sensing response between cracked MXene/PU fiber and plain core–sheath MXene/PU fiber.[120] (f) Sensing performance of MXene/PU fiber integrated fabric under repeated 1000 cycles bending. Reproduced with permission (d–f).[120] Copyright©2021, Elsevier.

applied and ΔP represents the applied pressure change.[116] For instance, Jialong An and his co-workers developed $Ti_3C_2T_x$-modified plain cotton fabric by simply dipping and drying techniques.[117] They observed that at low pressure (0–500 Pa), the sensitivity reached 19.78 K/Pa, whereas at relatively large pressure, 500–2000 Pa, the sensitivity was 6.11 K/Pa. This sensitivity decreased to 1.61 K/Pa even at high applied pressure. The reason behind this is that the conductive layer of MXene gets closer under small pressure, increasing the conductive path and so the sensitivity. However, at higher pressure, the conductive path seems to saturate which increases low conductivity, thus increasing low sensitivity. The phenomena of decreasing sensitivity with increased external pressure have also been seen in another study, where MXene-coated cotton fabric was modified with silicon nanoparticles (MX@SiNPs) to obtain a superhydrophobic sensor device.[118] The sensitivity of the fabricated sensor device was 12.23 k/Pa at less than 13 kPa, while in the pressure region of 13 to 52 kPa, it decreased to 2.00 k/Pa. However, the sensitivity was slightly increased to 8.46 k/Pa in the pressure region of 52 to 75 kPa. This slight increase in pressure sensitivity may arise due to the aligned conductive path of MXene materials. In addition, the MX@SiNPs sensor demonstrated greater flexibility. Fig. 9(c) shows that the LED light became brighter when the sensor was subjected to external pressure, compression, bending, and torsion, however, the brightness reduced when the sensor was in a relaxed state. Ma *et al.* developed wearable, hydrophobic, and multifunctional MXene-decorated air-laid paper, followed by surface modification with poly(dimethylsiloxane) (PDMS).[119] The developed MXene-decorated wearable device was used to fabricate pressure sensors, which showed a high sensitivity of 5.78 k/Pa and a rapid response time (30–40 ms). Moreover, the sensor device

showed no obvious degradation up to 5000 pressure/release cycles, demonstrating its excellent cyclic stability.

Other wearable sensors. Besides the use of strain and pressure sensors of MXene-based textronics, there are also other applications, like gas sensors, humidity sensors, and so on. It is considered that MXene is the ideal material to fabricate gas sensor devices. As MXene has wide functional groups, gas absorption may occur at the active sites of the MXene surface by forming hydrogen bonds with the gaseous molecules, causing the resistance change.[19] Thus, the detection of gas molecules happens. For instance, Tang *et al.* developed MXene/polyurethane (PU) stretchable core–sheath fibers, by using wet-spinning and spray-coating methods to fabricate wearable gas sensor devices.[120] Fig. 9(d) shows that the core–sheath fiber detected acetone gas molecules in a wide range from ppb level to saturated acetone vapor.

Furthermore, to increase the adsorption of acetone molecules on the MXene/PU fiber surface, a cracked surface was created by stretching the fiber. It was noticed that the cracked MXene/PU fibers exhibited a 44% increase in sensing response than the flat core–sheath fiber. Fig. 9(e) demonstrates the higher sensing response of cracked MXene/PU fibers than the core–sheath fibers. To evaluate the wearability of MXene/PU sensor fibers, it was knitted into a fabric, and it was seen that the fabric sensor showed a high flexibility by maintaining its sensing response during bending-relaxing for 1000 cycles, as shown in Fig. 9(f). This high sensitivity of acetone was attributed to the interaction of acetone and MXene nanomaterials *via* hydrogen bonding, resulting in charge transfer and resistance change. Lee *et al.* fabricated MXene/graphene hybrid fibers by wet-spinning technique to detect ammonia (NH_3) gas.[121] The fabricated fiber sensor showed an excellent sensing performance (6.77%), which was superior to individual MXene and graphene-based sensors. Moreover, the hybrid fiber was woven into a lab coat, which exhibited a remarkable gas response of 7.21% under exposure to 100 ppm NH_3 gas, which proved the possible application for a wearable NH_3 gas sensor device. Besides the developing wearable gas sensor device, MXene-based textronics are also widely used for humidity sensors. For instance, Liu *et al.* developed a vacuum-assisted layer-by-layer assembly technique to deposit electrically conductive substances (AgNW, and MXene) on silk textiles.[122] Moreover, the developed conductive fabric showed the change in electrical resistance under different moisture conditions, which ensures its potential application to detect human humidity (*i.e.* sweating levels) to monitor human health. Furthermore, the MXene-modified silk textile showed stable and repeatable resistance changes under the cyclic testing, indicating the stable sensitivity and durability to moisture.

Conclusions and future perspectives

In summary, there are numerous applications of MXene-based textronics, including wearable sensors, wearable electromagnetic shielding efficiency, wearable supercapacitors, and many more. In addition, to enhance the functional properties, numerous approaches are followed. Considering the applications, MXene-based fibers or yarns and fabrics are widely developed by taking advantage of different fabrication approaches, such as wet-spinning, electrospinning, coating, biscrolling, and so on. For MXene-based wearable electronic applications, these approaches are becoming popular gradually. However, there are still some challenges behind the development of MXene-based textronics. Based on our knowledge, the following aspects can be carefully considered for future research trends:

(i) The oxidation problem of MXene is one of the main reasons hindering the practical applications of MXene-based textronics because MXene-modified fabrics must be exposed to an open environment when it will be worn on the human body. Therefore, there is a huge possibility of occurring MXene oxidation. For this reason, for practical applications of MXene-based textronics, this major issue should be carefully considered. To solve this problem, annealing of MXene nanomaterials at high temperatures has been conducted recently. However, requiring high temperatures for annealing may impede the scalable fabrication of MXene-based textronics. Moreover, regarding the fabrication of textronics, coating hydrophobic materials (*e.g.* silicon, others) can also restrict the MXene nanosheets to exposure in the open environment. Although it should be ensured that conductivity should not be adversely affected.

(ii) Regarding the fabrication of wearable MXene-based textronics, conductive yarn may be the best option, as producing wearable electronic fabrics from MXene-modified conductive yarn is more scalable than modifying the fabric surface with MXene materials. There are some existing techniques, like wet-spinning, electrospinning, and coating, to fabricate conductive yarn. However, maintaining the electrical conductivity and mechanical strength simultaneously is still challenging. For instance, regarding the wet-spinning approach, introducing Ca^{2+} ions in the coagulation bath increases the yarn toughness. However, this type of approach is still limited.

(iii) Before the fabrication of MXene-based textronics by electrospinning, wet-spinning, coating, *etc.*, it is necessary to prepare the MXene solution. For this reason, different solvents such as water, dimethyl sulfoxide (DMSO), *n*-methyl pyrrolidone (NMP) as well as different organic solvents are used frequently. Moreover, the solvent mixture also ensures the surface modification of MXene nanomaterials which can contribute to the enhanced functional properties of MXene-based textronics, like energy storage capacity, sensing properties, and so on. However, the rheological study of MXene nanomaterials in different solvents in order to fabricate smart textiles is still in the underdeveloping stage. Therefore, this issue should be addressed carefully in the future.

(iv) Several factors, including MXene sizes, additional functional materials with MXene nanoflakes, fiber types, and fabric types, are essential for the functional properties of MXene-based textronics. For this reason, cotton fiber may be the best option due to its high moisture permeability and softness characteristics. However, for soldier's body armor, high-strength fiber, such as aramid, is highly demandable. Moreover, where water resistance fiber is required, for instance,

diver, the modification of MXene-based textronics with hydrophobic materials should be ensured. For these reasons, carefully choosing the materials is very necessary.

(v) Last but not least, recently MXene-based textronics have been extensively used in ECG, EMG, and other medical diagnosing sectors. These skin-attachable electronic devices should not create any negative consequences for humans regarding flexibility and human comfort. Moreover, these devices should be reliable in data acquisition for long time use. Therefore, more and wider research is needed to achieve this vision.

Author contributions

Md. Reazuddin Repon: conceptualization, methodology, data collection, writing – original draft preparation, supervision, visualization, contents approval. Daiva Mikučionienė: resources, writing – reviewing and editing. Tamal Krishna Paul: data collection, software, writing – original draft preparation. Jehan Y. Al-Humaidi: data collection, writing – reviewing and editing. Mohammed M. Rahman: data collection, writing – reviewing and editing. Tarekul Islam: data collection, writing – reviewing and editing. Sharof Shukhratov: writing – reviewing and editing, visualization.

Conflicts of interest

There are no conflicts to declare.

Acknowledgements

This work was supported by the Princess Nourah Bint Abdulrahman University, Researchers Supporting Project Number (PNURSP2024R24), Princess Nourah Bint Abdulrahman University, Riyadh, Saudi Arabia.

Notes and references

1 K. Keum, J. W. Kim, S. Y. Hong, J. G. Son, S. Lee and J. S. Ha, *Adv. Mater.*, 2020, **32**, 2002180.
2 Q. Li, K. Dai, W. Zhang, X. Wang, Z. You and H. Zhang, *Digit. Signal Process.*, 2021, **113**, 103038.
3 J. Chen, X. Wen, X. Liu, J. Cao, Z. Ding and Z. Du, *Nano Energy*, 2021, **80**, 105446.
4 D. H. Lee, J. C. Yang, J. Y. Sim, H. Kang, H.-R. Kim and S. Park, *ACS Appl. Mater. Interfaces*, 2022, **14**, 31312–31320.
5 J. Li, P. Yang, X. Li, C. Jiang, J. Yun, W. Yan, K. Liu, H. J. Fan and S. W. Lee, *ACS Energy Lett.*, 2023, **8**, 1–8.
6 L. Gao, G. Zhang, B. Yu, Z. Qiao and J. Wang, *Measurement*, 2020, **166**, 108252.
7 S. Bhattacharjee, C. R. Macintyre, X. Wen, P. Bahl, U. Kumar, A. A. Chughtai and R. Joshi, *Carbon*, 2020, **166**, 148–163.
8 S. Bhattacharjee, R. Joshi, A. A. Chughtai and C. R. Macintyre, *Adv. Mater. Interfaces*, 2019, **6**, 1900622.
9 S. Ryu, P. Lee, J. B. Chou, R. Xu, R. Zhao, A. J. Hart and S.-G. Kim, *ACS Nano*, 2015, **9**, 5929–5936.
10 P. L. Mahapatra, A. K. Singh, B. Lahiri, T. K. Kundu, A. K. Roy, P. Kumbhakar and C. S. Tiwary, *ACS Appl. Mater. Interfaces*, 2022, **14**, 30343–30351.
11 K. Wu, L. Yu, C. Lei, J. Huang, D. Liu, Y. Liu, Y. Xie, F. Chen and Q. Fu, *ACS Appl. Mater. Interfaces*, 2019, **11**, 40685–40693.
12 P.-C. Hsu, X. Liu, C. Liu, X. Xie, H. R. Lee, A. J. Welch, T. Zhao and Y. Cui, *Nano Lett.*, 2015, **15**, 365–371.
13 R. M. A. P. Lima, J. J. Alcaraz-Espinoza, F. A. G. da Silva and H. P. de Oliveira, *ACS Appl. Mater. Interfaces*, 2018, **10**, 13783–13795.
14 C. Yeon, G. Kim, J. W. Lim and S. J. Yun, *RSC Adv.*, 2017, **7**, 5888–5897.
15 C. Zhang and V. Nicolosi, *Energy Storage Mater.*, 2019, **16**, 102–125.
16 M. Naguib, V. N. Mochalin, M. W. Barsoum and Y. Gogotsi, *Adv. Mater.*, 2014, **26**, 992–1005.
17 G. Deysher, C. E. Shuck, K. Hantanasirisakul, N. C. Frey, A. C. Foucher, K. Maleski, A. Sarycheva, V. B. Shenoy, E. A. Stach, B. Anasori and Y. Gogotsi, *ACS Nano*, 2020, **14**, 204–217.
18 M. Naguib, M. Kurtoglu, V. Presser, J. Lu, J. Niu, M. Heon, L. Hultman, Y. Gogotsi and M. W. Barsoum, *Adv. Mater.*, 2011, **23**, 4248–4253.
19 C. Ma, M. Ma, C. Si, X. Ji and P. Wan, *Adv. Funct. Mater.*, 2021, **31**, 2009524.
20 C. Jin and Z. Bai, *ACS Sens.*, 2022, **7**, 929–950.
21 W. Meng, X. Liu, H. Song, Y. Xie, X. Shi, M. Dargusch, Z.-G. Chen, Z. Tang and S. Lu, *Nano Today*, 2021, **40**, 101273.
22 Q. Wang, H. Zhang, J. Liu, S. Zhao, X. Xie, L. Liu, R. Yang, N. Koratkar and Z. Yu, *Adv. Funct. Mater.*, 2019, **29**, 1–10.
23 J. S. Meena, S. Bin Choi, S.-B. Jung and J.-W. Kim, *Appl. Mater. Today*, 2022, **29**, 101612.
24 J. Zhang, X. Wang, G. Hang, Y. Wei, H. Wang, S. He and Z. Liu, *ACS Appl. Electron. Mater.*, 2023, **5**, 4704–4725.
25 K. A. S. Usman, S. Qin, L. C. Henderson, J. Zhang, D. Y. Hegh and J. M. Razal, *Mater. Horiz.*, 2021, **8**, 2886–2912.
26 Y. Cheng, Y. Xie, H. Cao, L. Li, Z. Liu, S. Yan, Y. Ma, W. Liu, Y. Yue, J. Wang, Y. Gao and L. Li, *Chem. Eng. J.*, 2023, **453**, 139823.
27 N. Krifa, R. Zouari, W. Miled, N. Behary, J. Vieillard, M. Cheikhrouhou and C. Campagne, *Fibers Polym.*, 2021, **22**, 2782–2791.
28 C. B. Hatter, A. Sarycheva, A. Levitt, B. Anasori, L. Nataraj and Y. Gogotsi, *C*, 2020, **6**, 64.
29 L. Wang, M. Tian, Y. Zhang, F. Sun, X. Qi, Y. Liu and L. Qu, *J. Mater. Sci.*, 2020, **55**, 6187–6194.
30 X. Liu, X. Jin, L. Li, J. Wang, Y. Yang, Y. Cao and W. Wang, *J. Mater. Chem. A*, 2020, **8**, 12526–12537.
31 S. Zou, D. Li, C. He, X. Wang, D. Cheng and G. Cai, *ACS Appl. Mater. Interfaces*, 2023, **15**, 10994–11003.
32 L. Yang, F. Lin, F. Zabihi, S. Yang and M. Zhu, *Int. J. Biol. Macromol.*, 2021, **181**, 1063–1071.
33 X. Li, J. Hao, R. Liu, H. He, Y. Wang, G. Liang, Y. Liu, G. Yuan and Z. Guo, *Energy Storage Mater.*, 2020, **33**, 62–70.

34 G. Yin, Y. Wang, W. Wang and D. Yu, *Colloids Surf., A*, 2020, **601**, 125047.
35 F. Aziz and A. F. Ismail, *Mater. Sci. Semicond. Process.*, 2015, **39**, 416–425.
36 F. Zabihi, Y. Xie, S. Gao and M. Eslamian, *Appl. Surf. Sci.*, 2015, **338**, 163–177.
37 J. E. Bishop, J. A. Smith and D. G. Lidzey, *ACS Appl. Mater. Interfaces*, 2020, **12**, 48237–48245.
38 Y. Zhang, Y. Wang, Q. Jiang, J. K. El-Demellawi, H. Kim and H. N. Alshareef, *Adv. Mater.*, 2020, **32**, 1908486.
39 S. Abdolhosseinzadeh, X. Jiang, H. Zhang, J. Qiu and C. Zhang, *Mater. Today*, 2021, **48**, 214–240.
40 M. Danish, M. Tayyab Raza, M. Iftikhar, I. Hassan, S. A. Husnain, M. Muneeb ul Hassan, M. Mumtaz, A. M. Khan, H. Noor and F. Shahzad, *Mater. Chem. Phys.*, 2024, **311**, 128573.
41 A. C. Mendhe, in *Simple Chemical Methods for Thin Film Deposition*, Springer Nature Singapore, Singapore, 2023, pp. 387–424.
42 S. Nandy and K. H. Chae, in *Ferrite Nanostructured Magnetic Materials*, Elsevier, 2023, pp. 309–334.
43 S. Ahn, T. Han, K. Maleski, J. Song, Y. Kim, M. Park, H. Zhou, S. Yoo, Y. Gogotsi and T. Lee, *Adv. Mater.*, 2020, **32**, 1–7.
44 D. B. Hall, P. Underhill and J. M. Torkelson, *Polym. Eng. Sci.*, 1998, **38**, 2039–2045.
45 M. A. K. Purbayanto, D. Bury, M. Chandel, Z. D. Shahrak, V. N. Mochalin, A. Wójcik, D. Moszczyńska, A. Wojciechowska, A. Tabassum, M. Naguib and A. M. Jastrzębska, *ACS Appl. Mater. Interfaces*, 2023, **15**, 44075–44086.
46 W. He, M. Sohn, R. Ma and D. J. Kang, *Nano Energy*, 2020, **78**, 105383.
47 C. Augello and H. Liu, Surface Modification of Magnesium and its Alloys for Biomedical Applications, *Elsevier*, 2015, **2**, 335–353.
48 B. S. Yilbas, A. Al-Sharafi and H. Ali, in *Self-Cleaning of Surfaces and Water Droplet Mobility*, Elsevier, 2019, pp. 45–98.
49 N. Bhardwaj and S. C. Kundu, *Biotechnol. Adv.*, 2010, **28**, 325–347.
50 J.-S. Park, *Adv. Nat. Sci.: Nanosci. Nanotechnol.*, 2010, **1**, 043002.
51 Y. Li, J. Zhu, H. Cheng, G. Li, H. Cho, M. Jiang, Q. Gao and X. Zhang, *Adv. Mater. Technol.*, 2021, **6**, 2100410.
52 Z.-M. Huang, Y.-Z. Zhang, M. Kotaki and S. Ramakrishna, *Compos. Sci. Technol.*, 2003, **63**, 2223–2253.
53 G. I. Taylor, *Proc. R. Soc. London, Ser. A*, 1969, **313**, 453–475.
54 A. S. Levitt, M. Alhabeb, C. B. Hatter, A. Sarycheva, G. Dion and Y. Gogotsi, *J. Mater. Chem. A*, 2019, **7**, 269–277.
55 X. Fu, L. Li, S. Chen, H. Xu, J. Li, V. Shulga and W. Han, *J. Colloid Interface Sci.*, 2021, **604**, 643–649.
56 E. A. Mayerberger, R. M. Street, R. M. McDaniel, M. W. Barsoum and C. L. Schauer, *RSC Adv.*, 2018, **8**, 35386–35394.
57 E. A. Mayerberger, O. Urbanek, R. M. McDaniel, R. M. Street, M. W. Barsoum and C. L. Schauer, *J. Appl. Polym. Sci.*, 2017, **134**, 45295.
58 W. Shao, M. Tebyetekerwa, I. Marriam, W. Li, Y. Wu, S. Peng, S. Ramakrishna, S. Yang and M. Zhu, *J. Power Sources*, 2018, **396**, 683–690.
59 A. Rohani Shirvan, A. Nouri and A. Sutti, *Eur. Polym. J.*, 2022, **181**, 111681.
60 S. Qin, K. A. S. Usman, D. Hegh, S. Seyedin, Y. Gogotsi, J. Zhang and J. M. Razal, *ACS Appl. Mater. Interfaces*, 2021, **13**, 36655–36669.
61 J. Zhang, S. Seyedin, S. Qin, Z. Wang, S. Moradi, F. Yang, P. A. Lynch, W. Yang, J. Liu, X. Wang and J. M. Razal, *Small*, 2019, **15**, 1–9.
62 B. Cheng and P. Wu, *ACS Nano*, 2021, **15**, 8676–8685.
63 L. Wang, M. Zhang, B. Yang and J. Tan, *ACS Appl. Mater. Interfaces*, 2021, **13**, 41933–41945.
64 L. Yue, M. Gong, J. Wang, S. Ma, Q. Chen, X. Kong, X. Lin, L. Zhang, Z. Wu and D. Wang, *ACS Mater. Lett.*, 2023, **5**, 2104–2113.
65 K. A. S. Usman, J. Zhang, S. Qin, Y. Yao, P. A. Lynch, P. Mota-Santiago, M. Naebe, L. C. Henderson, D. Hegh and J. M. Razal, *J. Mater. Chem. A*, 2022, **10**, 4770–4781.
66 S. Seyedin, E. R. S. Yanza and J. M. Razal, *J. Mater. Chem. A*, 2017, **5**, 24076–24082.
67 X. Zhao, J. Zhang, K. Lv, N. Kong, Y. Shao and J. Tao, *Carbon*, 2022, **200**, 38–46.
68 G. Wu, Z. Yang, Z. Zhang, B. Ji, C. Hou, Y. Li, W. Jia, Q. Zhang and H. Wang, *Electrochim. Acta*, 2021, **395**, 139141.
69 T. Zheng, X. Zhang, Y. Li, Y. Zhu, W. Yan, Z. Zhao, L. Zhang, C. Bai and X. Wang, *Mater. Lett.*, 2023, **336**, 133891.
70 W. Eom, H. Shin, R. B. Ambade, S. H. Lee, K. H. Lee, D. J. Kang and T. H. Han, *Nat. Commun.*, 2020, **11**, 2825.
71 T. Zhou, Y. Yu, B. He, Z. Wang, T. Xiong, Z. Wang, Y. Liu, J. Xin, M. Qi, H. Zhang, X. Zhou, L. Gao, Q. Cheng and L. Wei, *Nat. Commun.*, 2022, **13**, 4564.
72 H. Wu, Y. Zhang, A. L. Kjøniksen, X. Zhou and X. Zhou, *Adv. Funct. Mater.*, 2021, **31**, 1–38.
73 C. Yu, Y. Gong, R. Chen, M. Zhang, J. Zhou, J. An, F. Lv, S. Guo and G. Sun, *Small*, 2018, **14**, 1–7.
74 Z. Wang, S. Qin, S. Seyedin, J. Zhang, J. Wang, A. Levitt, N. Li, C. Haines, R. Ovalle-Robles, W. Lei, Y. Gogotsi, R. H. Baughman and J. M. Razal, *Small*, 2018, **14**, 1–9.
75 Y. Qian, J. Zhong and J. Ou, *Polym. Compos.*, 2023, **44**, 2581–2591.
76 Z. Ma, S. Kang, J. Ma, L. Shao, Y. Zhang, C. Liu, A. Wei, X. Xiang, L. Wei and J. Gu, *ACS Nano*, 2020, **14**, 8368–8382.
77 Y. Guan, W. Li, Y. Zhang, Z. Shi, J. Tan, F. Wang and Y. Wang, *Compos. Sci. Technol.*, 2017, **144**, 193–201.
78 X.-Y. Wang, S.-Y. Liao, Y.-J. Wan, H.-P. Huang, X.-M. Li, Y.-G. Hu, P.-L. Zhu, R. Sun and C.-P. Wong, *Mater. Today Phys.*, 2022, **23**, 100644.
79 S. K. Sinha, P. Bansal and S. Maity, *J. Inst. Eng.: Ser. E*, 2017, **98**, 71–78.

80 L.-Z. Huang, Q. Yuan, X.-X. Ji, D.-D. Li, W. Zhang, W.-Y. Guo, M.-Y. Qi and M.-G. Ma, *Cellulose*, 2022, **29**, 6997–7010.
81 W. Fan, Q. Wang, K. Rong, Y. Shi, W. Peng, H. Li, Z. Guo, B. Bin Xu, H. Hou, H. Algadi and S. Ge, *Nano-Micro Lett.*, 2024, **16**, 36.
82 Z.-G. Wang, F. Gong, W.-C. Yu, Y.-F. Huang, L. Zhu, J. Lei, J.-Z. Xu and Z.-M. Li, *Compos. Sci. Technol.*, 2018, **162**, 7–13.
83 K. Qian, Q. Zhou, S. Thaiboonrod, J. Fang, M. Miao, H. Wu, S. Cao and X. Feng, *J. Colloid Interface Sci.*, 2022, **613**, 488–498.
84 A. Hazarika, B. K. Deka, J. Seo, H. E. Jeong, Y. Bin Park and H. W. Park, *Nano Energy*, 2021, **86**, 106042.
85 J. Luo, S. Gao, H. Luo, L. Wang, X. Huang, Z. Guo, X. Lai, L. Lin, R. K. Y. Li and J. Gao, *Chem. Eng. J.*, 2021, **406**, 126898.
86 J. Yu, Z. Cui, J. Lu, J. Zhao, Y. Zhang, G. Fan, S. Liu, Y. He, Y. Yu and D. Qi, *Composites, Part B*, 2021, **224**, 109193.
87 Q. Li, R. Yin, D. Zhang, H. Liu, X. Chen, Y. Zheng, Z. Guo, C. Liu and C. Shen, *J. Mater. Chem. A*, 2020, **8**, 21131–21141.
88 A. Thakur, N. Chandran B.S., K. Davidson, A. Bedford, H. Fang, Y. Im, V. Kanduri, B. C. Wyatt, S. K. Nemani, V. Poliukhova, R. Kumar, Z. Fakhraai and B. Anasori, *Small Methods*, 2023, **7**, 2300030.
89 N. Driscoll, A. G. Richardson, K. Maleski, B. Anasori, O. Adewole, P. Lelyukh, L. Escobedo, D. K. Cullen, T. H. Lucas, Y. Gogotsi and F. Vitale, *ACS Nano*, 2018, **12**, 10419–10429.
90 M. Ghidiu, M. R. Lukatskaya, M.-Q. Zhao, Y. Gogotsi and M. W. Barsoum, *Nature*, 2014, **516**, 78–81.
91 K. Maleski, C. E. Ren, M.-Q. Zhao, B. Anasori and Y. Gogotsi, *ACS Appl. Mater. Interfaces*, 2018, **10**, 24491–24498.
92 N. He, S. Patil, J. Qu, J. Liao, F. Zhao and W. Gao, *ACS Appl. Energy Mater.*, 2020, **3**, 2949–2958.
93 Y.-Y. Peng, B. Akuzum, N. Kurra, M.-Q. Zhao, M. Alhabeb, B. Anasori, E. C. Kumbur, H. N. Alshareef, M.-D. Ger and Y. Gogotsi, *Energy Environ. Sci.*, 2016, **9**, 2847–2854.
94 H. Zhang, H. Ji, J. Chen, N. Wang and H. Xiao, *Ind. Crops Prod.*, 2022, **188**, 115653.
95 Y. Xu, Y. Tao, X. Zheng, H. Ma, J. Luo, F. Kang and Q. Yang, *Adv. Mater.*, 2015, **27**, 8082–8087.
96 K. Qin, J. Kang, J. Li, C. Shi, Y. Li, Z. Qiao and N. Zhao, *ACS Nano*, 2015, **9**, 481–487.
97 G. Chen, Y. Li, M. Bick and J. Chen, *Chem. Rev.*, 2020, **120**, 3668–3720.
98 H. Tang, Q. Hu, M. Zheng, Y. Chi, X. Qin, H. Pang and Q. Xu, *Prog. Nat. Sci.: Mater. Int.*, 2018, **28**, 133–147.
99 A. Levitt, S. Seyedin, J. Zhang, X. Wang, J. M. Razal, G. Dion and Y. Gogotsi, *Small*, 2020, **16**, 1–12.
100 X. Zhang, H. Chen and H. Zhang, *Chem. Commun.*, 2007, 1395–1405.
101 J. Yun, I. Echols, P. Flouda, Y. Chen, S. Wang, X. Zhao, D. Holta, M. Radovic, M. J. Green, M. Naraghi and J. L. Lutkenhaus, *ACS Appl. Mater. Interfaces*, 2021, **13**, 14068–14076.
102 F. Ye, B. Xu, R. Chen, R. Li and G. Chang, *J. Energy Storage*, 2023, **62**, 106803.
103 J. Li, J. Chen, H. Wang and X. Xiao, *ChemElectroChem*, 2021, **8**, 648–655.
104 T. He, H. Wang, J. Wang, X. Tian, F. Wen, Q. Shi, J. S. Ho and C. Lee, *Adv. Sci.*, 2019, **6**, 1901437.
105 T. La, S. Qiu, D. K. Scott, R. Bakhtiari, J. W. P. Kuziek, K. E. Mathewson, J. Rieger and H. Chung, *Adv. Healthcare Mater.*, 2018, **7**, 1801033.
106 Y. T. Tsukada, M. Tokita, H. Murata, Y. Hirasawa, K. Yodogawa, Y. Iwasaki, K. Asai, W. Shimizu, N. Kasai, H. Nakashima and S. Tsukada, *Heart Vessels*, 2019, **34**, 1203–1211.
107 M. R. Repon, D. Mikučionienė, R. Milašius, T. K. Paul, C. M. Ahmed, S. Z. Hussain and A. Haji, *Mater. Today Commun.*, 2023, **37**, 107251.
108 J. Wang, M. Shen, Z. Liu and W. Wang, *Nano Energy*, 2022, **97**, 107177.
109 M. Gong, L. Yue, J. Kong, X. Lin, L. Zhang, J. Wang and D. Wang, *ACS Appl. Mater. Interfaces*, 2021, **13**, 9053–9063.
110 X. Zhao, L.-Y. Y. Wang, C.-Y. Y. Tang, X.-J. J. Zha, Y. Liu, B.-H. H. Su, K. Ke, R.-Y. Y. Bao, M.-B. B. Yang and W. Yang, *ACS Nano*, 2020, **14**, 8793–8805.
111 D. Song, G. Ye, Y. Zhao, Y. Zhang, X. Hou and N. Liu, *ACS Nano*, 2022, **16**, 17168–17178.
112 G. He, L. Wang, X. Bao, Z. Lei, F. Ning, M. Li, X. Zhang and L. Qu, *Composites, Part B*, 2022, **232**, 109618.
113 X. Zhang, X. Wang, Z. Lei, L. Wang, M. Tian, S. Zhu, H. Xiao, X. Tang and L. Qu, *ACS Appl. Mater. Interfaces*, 2020, **12**, 14459–14467.
114 L. Yuan, M. Zhang, T. Zhao, T. Li, H. Zhang, L. Chen and J. Zhang, *Sens. Actuators, A*, 2020, **315**, 112192.
115 Z. Jia, Z. Li, S. Ma, W. Zhang, Y. Chen, Y. Luo, D. Jia, B. Zhong, J. M. Razal, X. Wang and L. Kong, *J. Colloid Interface Sci.*, 2021, **584**, 1–10.
116 Y. Xie, Y. Cheng, Y. Ma, J. Wang, J. Zou, H. Wu, Y. Yue, B. Li, Y. Gao, X. Zhang and C. Nan, *Adv. Sci.*, 2023, **10**, 2205303.
117 J. An, Y. Ma, M. He, J. Yan, C. Zhang, X. Li, P. Shen, S. Luo and Y. Gao, *Sens. Actuators, A*, 2020, **311**, 112081.
118 S. Wang, X. Du, Y. Luo, S. Lin, M. Zhou, Z. Du, X. Cheng and H. Wang, *Chem. Eng. J.*, 2021, **408**, 127363.
119 C. Ma, Q. Yuan, H. Du, M. G. Ma, C. Si and P. Wan, *ACS Appl. Mater. Interfaces*, 2020, **12**, 34226–34234.
120 Y. Tang, Y. Xu, J. Yang, Y. Song, F. Yin and W. Yuan, *Sens. Actuators, B*, 2021, **346**, 130500.
121 S. H. Lee, W. Eom, H. Shin, R. B. Ambade, J. H. Bang, H. W. Kim and T. H. Han, *ACS Appl. Mater. Interfaces*, 2020, **12**, 10434–10442.
122 L. X. Liu, W. Chen, H. Bin Zhang, Q. W. Wang, F. Guan and Z. Z. Yu, *Adv. Funct. Mater.*, 2019, **29**, 1–10.
123 A. Levitt, J. Zhang, G. Dion, Y. Gogotsi and J. M. Razal, *Adv. Funct. Mater.*, 2020, **30**, 1–22.
124 R. De Silva, K. Vongsanga, X. Wang and N. Byrne, *Cellulose*, 2016, **23**, 2741–2751.
125 A. Ahmed, M. M. Hossain, B. Adak and S. Mukhopadhyay, *Chem. Mater.*, 2020, **32**, 10296–10320.

126 J. Yan, Y. Ma, C. Zhang, X. Li, W. Liu, X. Yao, S. Yao and S. Luo, *RSC Adv.*, 2018, **8**, 39742–39748.
127 W. Zhao, Y. Zheng, J. Qian, Z. Zhaofa, Z. Jin, H. Qiu, C. Zhu and X. Hong, *J. Alloys Compd.*, 2022, **923**, 166471.
128 X. Liu, X. Du, L. Li, Y. Cao, Y. Yang, W. Wang and J. Wang, *Composites, Part A*, 2022, **156**, 106883.
129 H. Hwang, S. Byun, S. Yuk, S. Kim, S. H. Song and D. Lee, *Appl. Surf. Sci.*, 2021, **556**, 149710.
130 M. Jiang, D. Jiang, J. Wang, Y. Sun and J. Liu, *Chem. Eng. J.*, 2023, **459**, 141527.
131 X. Zheng, Y. Wang, W. Nie, Z. Wang, Q. Hu, C. Li, P. Wang and W. Wang, *Composites, Part A*, 2022, **158**, 106985.
132 X. Zheng, W. Nie, Q. Hu, X. Wang, Z. Wang, L. Zou, X. Hong, H. Yang, J. Shen and C. Li, *Mater. Des.*, 2021, **200**, 109442.
133 S. Uzun, S. Seyedin, A. L. Stoltzfus, A. S. Levitt, M. Alhabeb, M. Anayee, C. J. Strobel, J. M. Razal, G. Dion and Y. Gogotsi, *Adv. Funct. Mater.*, 2019, **29**, 1905015.
134 J. V. Vaghasiya, C. C. Mayorga-Martinez, J. Vyskočil and M. Pumera, *Biosens. Bioelectron.*, 2022, **205**, 114092.
135 J. Zhang, X. Wang, G. Hang, W. Zhang, Z. Zheng, J. Duan and Z. Liu, *Compos. Commun.*, 2024, **45**, 101817.
136 X. Xu, S. Wang, H. Wu, Y. Liu, F. Xu and J. Zhao, *Colloids Surf., B*, 2021, **207**, 111979.
137 M. A. K. Purbayanto, M. Jakubczak, D. Bury, V. G. Nair, M. Birowska, D. Moszczyńska, A. Jastrzębska, M. Abiyyu, K. Purbayanto, M. Jakubczak, D. Bury, V. G. Nair, A. Jastrz, M. Birowska and D. Moszczyn, *ACS Appl. Nano Mater.*, 2022, **5**, 5373–5386.
138 X. Liu, J. Miao, Q. Fan, W. Zhang, X. Zuo, M. Tian, S. Zhu, X. Zhang and L. Qu, *ACS Appl. Mater. Interfaces*, 2021, **13**, 56607–56619.
139 B. Yan, M. Zhou, Y. Yu, B. Xu, L. Cui, Q. Wang and P. Wang, *Composites, Part A*, 2022, **160**, 107038.
140 X. Wang, Y. Tao, S. Pan, X. Fang, C. Lou, Y. Xu, J. Wu, M. Sang, L. Lu, X. Gong, T. Luo and S. Xuan, *npj Flexible Electron.*, 2022, **6**, 95.
141 M. Chao, P. Di, Y. Yuan, Y. Xu, L. Zhang and P. Wan, *Nano Energy*, 2023, **108**, 108201.